Leaf Shrinkage with Dehydration: Coordination with Hydraulic Vulnerability and Drought Tolerance[1][C][W][OPEN]

Christine Scoffoni*, Christine Vuong, Steven Diep, Hervé Cochard, and Lawren Sack

Department of Ecology and Evolutionary Biology, University of California, Los Angeles, California 90095 (C.S., C.V., S.D., L.S.); and Institut National de la Recherche Agronomique, Unité Mixte de Recherche 547, Laboratoire Physique et Physiologie Integratives de l'Arbre Fruitier et Forestier, F–63100 Clermont-Ferrand, France (H.C.)

Leaf shrinkage with dehydration has attracted attention for over 100 years, especially as it becomes visibly extreme during drought. However, little has been known of its correlation with physiology. Computer simulations of the leaf hydraulic system showed that a reduction of hydraulic conductance of the mesophyll pathways outside the xylem would cause a strong decline of leaf hydraulic conductance (K_{leaf}). For 14 diverse species, we tested the hypothesis that shrinkage during dehydration (i.e. in whole leaf, cell and airspace thickness, and leaf area) is associated with reduction in K_{leaf} at declining leaf water potential (Ψ_{leaf}). We tested hypotheses for the linkage of leaf shrinkage with structural and physiological water relations parameters, including modulus of elasticity, osmotic pressure at full turgor, turgor loss point (TLP), and cuticular conductance. Species originating from moist habitats showed substantial shrinkage during dehydration before reaching TLP, in contrast with species originating from dry habitats. Across species, the decline of K_{leaf} with mild dehydration (i.e. the initial slope of the K_{leaf} versus Ψ_{leaf} curve) correlated with the decline of leaf thickness (the slope of the leaf thickness versus Ψ_{leaf} curve), as expected based on predictions from computer simulations. Leaf thickness shrinkage before TLP correlated across species with lower modulus of elasticity and with less negative osmotic pressure at full turgor, as did leaf area shrinkage between full turgor and oven desiccation. These findings point to a role for leaf shrinkage in hydraulic decline during mild dehydration, with potential impacts on drought adaptation for cells and leaves, influencing plant ecological distributions.

As leaves open their stomata to capture CO_2 for photosynthesis, water is lost to transpiration, which needs to be replaced by flow through the hydraulic system. The leaf hydraulic system has two components, which act essentially in series: the pathways for water movement through the xylem from the petiole to leaf minor veins, and those through the living bundle sheath and mesophyll cells to the sites of evaporation (Tyree and Zimmermann, 2002; Sack et al., 2004; Sack and Holbrook, 2006). The decline in leaf hydraulic conductance (K_{leaf}) with dehydration may thus depend on both components. The importance of the xylem component is well established. Vein xylem embolism and cell collapse have been observed in dehydrating leaves (Salleo et al.,

2001; Cochard et al., 2004a; Johnson et al., 2009), and computer modeling and experimental work showed that species with high major vein length per leaf area (VLA; i.e. for the first three vein-branching orders) were more resistant to hydraulic decline, providing more pathways around embolisms (Scoffoni et al., 2011). However, the physical impacts of dehydration on the extraxylem pathways have not been studied, even though in turgid leaves these pathways account for 26% to 88% of leaf hydraulic resistance (i.e. of $1/K_{leaf}$), depending on species (Sack et al., 2003a; Cochard et al., 2004b). The aim of this study was to determine whether leaf shrinkage during dehydration relates to the decline of K_{leaf} as well as the structural determinants of leaf shrinkage.

The shrinkage of leaves with dehydration has drawn attention for over 100 years. Leaves shrink in their area (Bogue, 1892; Gardner and Ehlig, 1965; Jones, 1973; Tang and Boyer, 2007; Blonder et al., 2012) and, considered in relative terms, even more strongly in their thickness (Fig. 1; Meidner, 1952; Gardner and Ehlig, 1965; Downey and Miller, 1971; Syvertsen and Levy, 1982; Saini and Rathore, 1983; Burquez, 1987; McBurney, 1992; Sancho-Knapik et al., 2010, 2011). Leaves fluctuate in thickness daily and seasonally according to transpiration (Kadoya et al., 1975; Tyree and Cameron, 1977; Fensom and Donald, 1982; Rozema et al., 1987; Ogaya and Peñuelas, 2006; Seelig et al., 2012). Indeed, the relation of leaf thickness to water status is so tight that using leaf thickness to guide irrigation has led to water savings of up to 45% (Seelig et al., 2012).
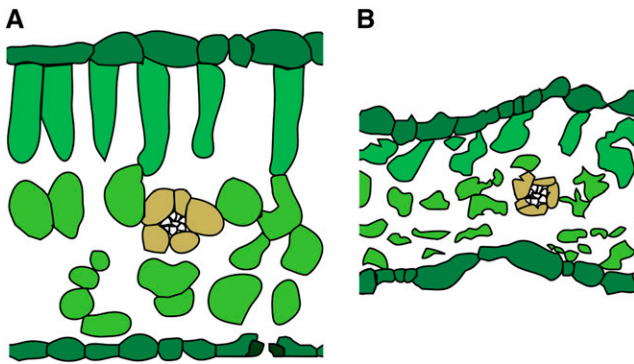
Figure 1. Sketches of a fully turgid leaf (A) versus a strongly dehydrated leaf (B; drawings based on leaf cross sections of sunflower in Fellows and Boyer, 1978). Note the strong reduction in leaf thickness, cell thickness, and intercellular airspaces in the dehydrated leaf. Epidermal cells are shrunk in the dehydrated leaf, inducing whole-leaf area shrinkage. Note that this sketch represents shrinkage for a typical drought-sensitive species. Many species such as oaks (*Quercus* spp.) will experience less thickness shrinkage and an increase in intercellular airspace (see "Discussion"). [See online article for color version of this figure.]

Previous studies of leaf shrinkage with progressive dehydration have tended to focus on single or few species. These studies showed that thickness declines with water status in two phases. Before the bulk leaf turgor loss point (TLP; leaf water potential [Ψ_{leaf}] at TLP) is reached, the slope of leaf thickness versus Ψ_{leaf} or relative water content (RWC) is shallower than past TLP for most species (Meidner, 1955, Kennedy and Booth, 1958, Burquez, 1987, McBurney, 1992, Sancho-Knapik et al., 2010, 2011). This is because before TLP, declining Ψ_{leaf} is strongly driven by declines in turgor pressure, which have a relatively low impact on cell and airspace volume, whereas past the TLP, declining Ψ_{leaf} depends only on solute concentration, which increases in inverse proportion as cell water volume declines while airspaces may shrink or expand (Tyree and Hammel, 1972, Sancho-Knapik et al., 2011). However, the steepness of the slope of leaf thickness versus Ψ_{leaf} before TLP seems to vary strongly across species (Meidner, 1955; Kennedy and Booth, 1958; Fellows and Boyer, 1978; Burquez, 1987; Colpitts and Coleman, 1997; Sancho-Knapik et al., 2010).

A high leaf cell volume and turgor is crucial to physiological processes (Boyer, 1968; Lawlor and Cornic, 2002). Shrinkage may affect cell connectivity and water transport (Sancho-Knapik et al., 2011). However, no studies have tested for a possible relationship of leaf shrinkage with the decline of K_{leaf} during dehydration. Such an association would arise if, across species, shrinkage occurred simultaneously with vein xylem embolism or if tissue shrinkage led to declines in the extraxylem hydraulic conductance.

To refine our hypotheses, we modified a computer model of the leaf hydraulic system (Cochard et al., 2004b; McKown et al., 2010; Scoffoni et al., 2011) to predict the impact of losses of xylem and extraxylem conductance

on the response of K_{leaf} to dehydration. We characterized the degree of leaf shrinkage in thickness, in the thickness of cells and airspaces within the leaf, and in leaf area for 14 species diverse in phylogeny, leaf traits, and drought tolerance. We hypothesized that loss of extraxylem hydraulic conductance should have a greater impact on K_{leaf} at less negative water potentials when xylem tensions are too weak to trigger embolism and induce dramatic declines in K_{leaf}. We hypothesized that species with greater degrees of shrinkage before TLP would experience greater loss of K_{leaf}. Furthermore, we hypothesized that species from moist habitats would have greater degrees of shrinkage.

For insight into the mechanisms and consequences of leaf shrinkage, we also investigated the relationships of 18 indices of leaf shrinkage with a wide range of aspects of leaf structure and composition, including gross morphology, leaf venation architecture, parameters of pressure-volume curves, and leaf water storage. We hypothesized that, across species, shrinkage in whole leaf, cell, and intercellular airspace thickness would be lower for species with greater allocation to structural rigidity and osmotic concentration, and thus shrinkage would be positively correlated with a lower modulus of elasticity (ε), less negative osmotic pressure at full turgor (π_o), lower leaf mass per area (LMA), and lower leaf density. Additionally, we tested the longstanding hypothesis that species with higher major VLA and/or minor VLA (i.e. the fourth and higher vein-branching orders) would shrink less in area and/or thickness with dehydration (Gardner and Ehlig, 1965). Finally, we tested the ability of dehydrated leaves to recover in size with rehydration. We hypothesized that recovery would be greater for mildly than for strongly dehydrated leaves and that species with greater leaf shrinkage would be better able to recover from shrinkage.

RESULTS

Computer Simulations Demonstrate the Potential Importance of Extraxylem Hydraulic Decline

We used computer simulation modeling with K_leaf version 6.1 (Cochard et al., 2004b; McKown et al., 2010; Scoffoni et al., 2011) to determine the impact of vulnerability of the outside-xylem mesophyll pathways in driving the decline of K_{leaf} with dehydration (Fig. 2; Table I; Supplemental Table S1). We generated eight leaf hydraulic vulnerability curves based on different assumptions about the distribution of hydraulic resistance and vulnerability characteristics of various components of the flow pathway. We considered two general cases: (1) most hydraulic resistance was within the outside-xylem component (i.e. the outside xylem hydraulic resistance [R_{ox}] > the xylem hydraulic resistance [R_x]); or, conversely, (2) R_x > R_{ox}. For each of these two general cases, we considered four vulnerability scenarios: (1) low vulnerability for xylem and outside-xylem components; (2) high vulnerability for only the outside-xylem component; (3) high vulnerability for only the xylem
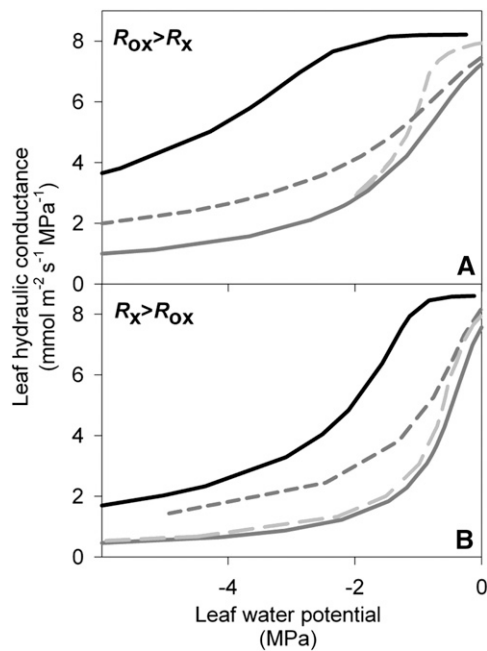
Figure 2. Computer-simulated leaf hydraulic vulnerability curves indicating the theoretical impact of reducing hydraulic conductance in the within-xylem and outside-xylem components for leaves with high and low resistance outside the xylem (A and B, respectively). Simulations were run for leaves with: (1) low vulnerability for xylem and outside-xylem components (P_{50} for the vulnerability of each component = -1 MPa; black line), (2) high vulnerability for only the outside-xylem component ($P_{50} = -1$ and -0.25 MPa for the within-xylem and outside-xylem components, respectively; dark gray dashed line), (3) high vulnerability for only the xylem component ($P_{50} = -0.25$ and -1 MPa for the within-xylem and outside-xylem components, respectively; light gray dashed line), and (4) high vulnerability for both the xylem and outside-xylem components ($P_{50} = -0.25$ MPa; gray solid line).

component; and (4) high vulnerability for the xylem and outside-xylem components (for additional details and parameterization of each scenario, see "Materials and Methods"). Although the vulnerability of the xylem in given vein orders and in the mesophyll was specified in the K_leaf model by a two-parameter sigmoidal function (Pammenter and Vander Willigen, 1998; see "Materials and Methods"), in all modeled scenarios a three-parameter logistic function was selected by maximum likelihood for the leaf vulnerability curve; the emergent whole-leaf response differed in structure from that specified for its components (Supplemental Table S1).

Consistent with expectations, the simulations showed that whole leaves were most vulnerable when both xylem and outside-xylem mesophyll components were vulnerable. The outside-xylem vulnerability had a substantial impact on K_{leaf} vulnerability. Simulating a greater vulnerability to dehydration in only the outside-xylem component or only the xylem led to substantially less negative water potential at 50% and 80% loss of K_{leaf} (P_{50} and P_{80}) and steeper initial slopes than when simulating

a low xylem and outside-xylem vulnerability (Fig. 2, A and B, compare light or dark gray dashed lines with black solid lines; Table I). Furthermore, because the outside-xylem mesophyll component is a terminal hydraulic bottleneck, it is critical for protection of the xylem component. Across simulations, P_{50} was always considerably more negative than the pressure inside the xylem at P_{50} (2- to 8-fold more negative; Table I). At given input values for the within-xylem and outside-xylem vulnerability, the leaf was less vulnerable when more hydraulic resistance was found outside the xylem (i.e. $R_{ox} > R_x$ rather than $R_x > R_{ox}$), with more negative P_{50} and P_{80} values and vulnerability curves with shallower slopes (Table I; Fig. 2).

Furthermore, the outside-xylem vulnerability played the greatest role in driving the initial vulnerability at mild water deficits. The initial slope of the vulnerability curve (before the bulk of cavitation would occur) was steeper when the outside-xylem component was vulnerable than when only the xylem component was vulnerable (Fig. 2, A and B, compare gray dashed and light gray dashed lines; Table I) and similar to that found when both xylem and outside-xylem components were vulnerable (Fig. 2, compare gray dashed with gray solid lines; Table I). By contrast, the behavior of the leaf vulnerability curve at stronger water deficits was strongly influenced by the xylem component; thus, the P_{80} values when both xylem and outside-xylem components were vulnerable were similar to that found in the simulation when only the xylem was vulnerable, substantially less negative than when only the outside-xylem was vulnerable (Fig. 2; Table I). There was less difference across simulations in the P_{50} values (Table I).

These findings indicated a strong impact of reduction in mesophyll hydraulic conductance on K_{leaf} vulnerability, especially at high water potentials, with more pronounced effects of xylem embolism on K_{leaf} vulnerability under stronger dehydration (Fig. 2; Table I).

Leaf Shrinkage with Dehydration: Variation across Diverse Species

Species varied significantly in their leaf shrinkage with dehydration (Fig. 3) and in all nine key leaf shrinkage parameters (one-way ANOVA, $P < 0.001$; Tables II–V; Supplemental Table S2; for additional parameters that were correlated with the nine key parameters, see Supplemental Tables S2–S4 and Supplemental Results S1). Species varied 18-fold in the slope of thickness against Ψ_{leaf} before TLP ($dT_{leaf}/d\Psi$), from -31% MPa^{-1} for *Platanus racemosa*, which had slopes of cell and airspace thickness against Ψ_{leaf} before TLP ($dT_C/d\Psi$ and $dT_A/d\Psi$, respectively) of -10% and -60% MPa^{-1}, respectively, to -1.7% MPa^{-1} for *Quercus agrifolia* ($dT_C/d\Psi$ and $dT_A/d\Psi$ of -4.9 and -3.9, respectively). The $dT_C/d\Psi$ varied 3-fold across species, from -4.1% MPa^{-1} for *Cercocarpus betuloides* to -13% MPa^{-1} for *Bauhinia galpinii*, and $dT_A/d\Psi$ was even more variable, ranging from an increase in airspace of 3.9% MPa^{-1} for *Q. agrifolia* to a reduction of airspace of 60% MPa^{-1} for *P. racemosa*.

Table I. *Results from model simulations testing the impacts on leaf hydraulic vulnerability of declines in conductivity in the xylem and outside-xylem pathways*

For each set of simulations, we present R_{ox}, xylem P_{50} and outside-xylem P_{50}, K_{max}, Ψ_{leaf} at leaf P_{50} and leaf P_{80}, P_{xylem} at leaf P_{50}, and the initial

slope of the leaf hydraulic vulnerability curve (at -0.1 MPa), obtained from the logistic function $\left(K_{leaf} = \dfrac{a}{1+\left(\frac{\Psi_{leaf}}{x_0}\right)^b}\right)$, which was selected as the

maximum likelihood model in all simulations (compare with Supplemental Table S1).

Scenario	Simulations	Input Conditions				Output of Leaf-Level Responses			
		R_{ox}	Xylem P_{50}	Outside-Xylem P_{50}	K_{max}	Leaf P_{50}	Leaf P_{80}	P_{xylem} at P_{50}	Initial Slope
		%		MPa	mmol m^{-2} s^{-1} MPa^{-1}		MPa		mmol m^{-2} s^{-1} MPa^{-2}
$R_{ox} > R_x$	Low vulnerability for xylem and outside-xylem components	74	-1.00	-1.00	8.62	-5.50	-11.6	-0.74	-0.09
	High vulnerability for only the outside-xylem component	76	-1.00	-0.25	7.56	-2.37	-7.78	-0.28	-2.08
	High vulnerability for only the xylem component	71	-0.25	-1.00	8.18	-1.53	-2.72	-0.32	-0.28
	High vulnerability for xylem and outside-xylem components	74	-0.25	-0.25	7.26	-1.48	-3.83	-0.25	-1.97
$R_x > R_{ox}$	Low vulnerability for xylem and outside-xylem components	39	-1.00	-1.00	9.03	-2.49	-5.03	-0.78	-0.32
	High vulnerability for only the outside-xylem component	42	-1.00	-0.25	8.32	-1.23	-3.92	-0.35	-4.50
	High vulnerability for only the xylem component	36	-0.25	-1.00	8.02	-0.83	-1.78	-0.39	-3.06
	High vulnerability for xylem and outside-xylem components	39	-0.25	-0.25	7.65	-0.68	-1.75	-0.30	-6.02

The maximum shrinkage in thickness (PLT_{dry}; i.e. that observed in a dry leaf relative to a fully turgid leaf) varied 4-fold across species, from 23% for *Q. agrifolia* to 83% for *B. galpinii* (Table V). Notably, the proportion of the leaf thickness constituted of cell versus air did not shift significantly between full turgor and TLP. Across species, the mean $\pm$ SE for the percentage of cell and air thickness at full turgor were 67% $\pm$ 4% and 33% $\pm$ 4%, respectively, very similar to those at TLP ($PT_{C,TLP}$ and $PT_{A,TLP}$), 69% $\pm$ 5% and 31% $\pm$ 5%, respectively (paired Student's *t* tests, *P* = 0.44–0.49; Supplemental Table S2).

The coordination of leaf thickness shrinkage with TLP also varied strongly across species. The percentage loss of leaf thickness at turgor loss point ($PLT_{leaf,TLP}$) varied 8-fold among species, from 4.6% for *Raphiolepis indica* to 38% for *Lantana camara* (Table V). The cell shrinkage at turgor loss point ($PLT_{C,TLP}$) varied 2-fold among species, from 11% for *C. betuloides* to 21% for *Camellia sasanqua*, and the intercellular airspace shrinkage at turgor loss point ($PLT_{A,TLP}$) ranged from a gain in airspace in the leaf of 12% for *Q. agrifolia* to a loss of airspace of up to 77% for *L. camara* (Table V). Species differences in $PLT_{leaf,TLP}$ were driven by variation in $PLT_{A,TLP}$ rather than $PLT_{C,TLP}$; there was a tight correlation of $PLT_{leaf,TLP}$ with $PLT_{A,TLP}$ (Spearman rank correlation [r_s] = 0.94, Pearson correlation [r_p] = 0.96, *P* < 0.001) but not with $PLT_{C,TLP}$ (*P* > 0.05).

Percentage shrinkage in leaf area was much lower than that for thickness. Percentage loss of area at TLP ($PLA_{leaf,TLP}$) ranged from 0.5% for *B. galpinii* to 14% for sunflower (*Helianthus annuus*; Table V). The percentage loss of area in a dry leaf (PLA_{dry}; i.e. that for a dry

leaf) ranged 14-fold across species, from 4.9% for *Heteromeles arbutifolia* to 69% for sunflower (Table V).

Species native to moist habitats experienced more shrinkage in thickness and area than species from dry habitats (for more details, see Supplemental Results S2).

Coordination of Leaf Shrinkage Responses and Leaf Hydraulic Vulnerability

Across species, $dT_{leaf}/d\Psi$ and $dT_C/d\Psi$ correlated with the slope of the leaf hydraulic vulnerability curve at $\Psi_{leaf} = -0.5$ MPa ($dK_{leaf}/d\Psi$) and with P_{50} and P_{80} (Fig. 4; Supplemental Table S3). No significant correlations were found between the slope of the shrinkage curve for the intercellular airspaces and $dK_{leaf}/d\Psi$, P_{50}, or P_{80} (Fig. 4; Supplemental Table S3). Species with greater PLT_{dry} tended to have higher maximum K_{leaf} (K_{max}; Pearson and Spearman coefficients r_p and r_s = 0.65 and 0.68, respectively, *P* < 0.05; Supplemental Table S3) and also experienced steeper $dK_{leaf}/d\Psi$ (r_p and r_s = 0.76–0.88, *P* < 0.05; Supplemental Table S3). No correlations were found between K_{leaf} at TLP and leaf shrinkage traits ($|r_p|$ and $|r_s|$ = 0.02–0.42, *P* > 0.05; Supplemental Table S3).

Recovery from shrinkage in thickness for leaves dehydrated before TLP was high but not complete, ranging from 60% in *Magnolia grandiflora* to 99% in *Romneya coulterii* (Supplemental Table S5). For eight of 10 species tested, a similar recovery was found for leaves that had been dehydrated to before or past TLP (Supplemental Table S5; Supplemental Results S3).

Figure 3. Plots of leaf thickness shrinkage versus Ψ_{leaf} for 14 species of diverse leaf form and texture and drought tolerance; a typical plot is presented for each species. The blue shaded areas represent the thickness of the cells, and the white areas represent the thickness of the intercellular airspace. The gray horizontal lines represent the maximum shrinkage in leaf thickness (i.e. for an oven-dried leaf). The red vertical lines represent TLP, and the red horizontal lines represent the thickness of the leaf at TLP. Species are ordered top left to bottom right from lowest to highest ε. Due to area wrinkling with dehydration of sunflower, *M. grandiflora*, and *S. canariensis*, the cell and airspace thickness could not be estimated, and only the whole-leaf shrinkage is shown in light blue (see "Materials and Methods"). [See online article for color version of this figure.]
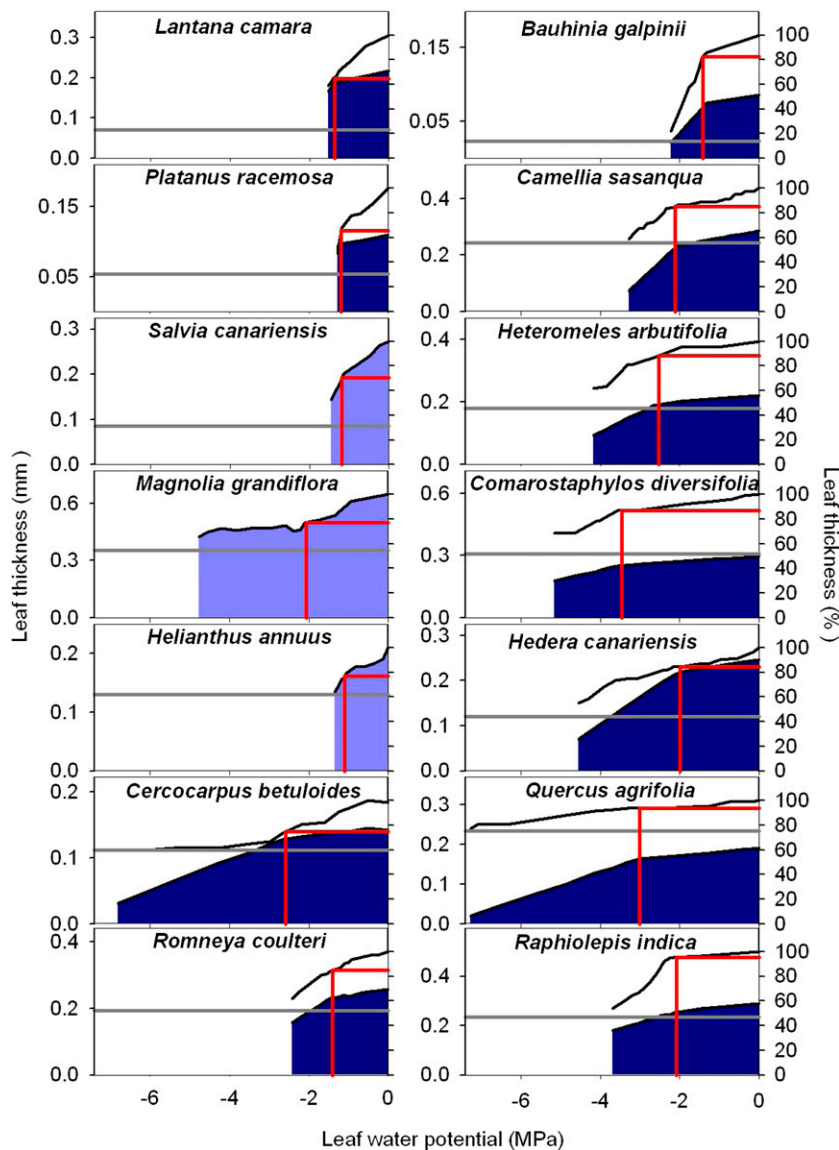
Correlation of Leaf Shrinkage with Leaf Pressure-Volume Parameters, Water Storage, Structure, Venation Architecture, and Cuticular Conductance

Across species, thickness shrinkage correlated with pressure-volume curve parameters (Fig. 5, A–C), which themselves were strongly intercorrelated (Fig. 5, F–O; Supplemental Table S3). Species with more negative π_o and osmotic pressure at TLP (π_{TLP}) and higher ε shrank less in thickness before TLP and tended to have shallower $dT_{leaf}/d\Psi$, $dT_C/d\Psi$, and $dT_A/d\Psi$ (r_p and r_s = 0.62–0.86, $P < 0.05$; Supplemental Table S3). Leaf area shrinkage also related to pressure-volume parameters. A high $PLA_{leaf,TLP}$ correlated with low ε (r_p and r_s = −0.62 to −0.68, $P < 0.05$; Supplemental Table S3). PLA_{dry} correlated with high π_o and π_{TLP} and low ε ($|r_p|$ and $|r_s|$ = 0.80–0.83, $P < 0.001$; Fig. 6; Supplemental Table S3).

Notably, due to the strong relationship between ε (MPa) and PLA_{dry} (%), a fitted power law equation could be used to estimate ε from PLA_{dry} ($r^2 = 0.66$, $P < 0.001$):

$$\varepsilon = 41.4 \times PLA_{dry}^{-0.522} \qquad (1)$$

Leaf shrinkage traits also correlated with water storage traits. With few exceptions, the magnitudes of $dT_{leaf}/d\Psi$, $dT_C/d\Psi$, and $dT_A/d\Psi$ correlated with leaf capacitances (amount of water storage) at full turgor and TLP and with saturated water content (capacitance at full turgor [C_{FT}], capacitance at π_{TLP} [C_{TLP}], and saturated water content [SWC]; r_p and r_s values up to 0.93, $P < 0.05$; Supplemental Table S3). The PLA_{dry} was positively correlated with C_{FT}, C_{TLP}, SWC, and leaf area-specific C_{TLP} (C^*_{TLP}; r_p and r_s = 0.55–0.86, $P < 0.05$; Supplemental Table S3).

Across species, leaf shrinkage also related to leaf structure. The $PLT_{leaf,TLP}$ correlated negatively with LMA and

Table II. *Study species, family, and mean ± SE for leaf thickness, area, mass per area, and pressure-volume parameters*

Species	Family	Plant Habit	Leaf Thickness at Full Turgor (mm)	Leaf Area (cm²)	LMA (g m⁻²)	π_o (MPa)	π_{TLP} (MPa)	ε	RWC at TLP (%)
Moist habitat									
B. galpinii	Fabaceae	Shrub	0.17 ± 0.007	22.2 ± 1.44	45.0 ± 1.60	-1.15 ± 0.08	-1.41 ± 0.07	7.81 ± 1.61	81.4 ± 3.39
C. sasanqua[a]	Theaceae	Shrub	0.40 ± 0.01	12.8 ± 0.98	178 ± 9.08	-1.61 ± 0.13	-2.12 ± 0.18	7.98 ± 1.11	76.7 ± 3.35
Helianthus annuus[a]	Asteraceae	Herb	0.20 ± 0.01	101 ± 6.61	31.2 ± 1.06	-0.87 ± 0.12	-1.09 ± 0.12	5.49 ± 0.79	84.4 ± 1.50
L. camara[a]	Verbenaceae	Shrub	0.29 ± 0.01	16.8 ± 1.22	61.4 ± 4.18	-1.10 ± 0.04	-1.37 ± 0.04	4.85 ± 0.33	78.0 ± 2.30
M. grandiflora[a]	Magnoliaceae	Tree	0.63 ± 0.04	77.2 ± 7.12	220 ± 11.0	-1.42 ± 0.02	-2.06 ± 0.05	13.3 ± 1.31	89.3 ± 1.20
P. racemosa[a]	Platanaceae	Tree	0.17 ± 0.01	130 ± 14.4	56.3 ± 2.34	-0.93 ± 0.08	-1.19 ± 0.09	7.09 ± 0.25	87.0 ± 1.44
R. indica[a]	Rosaceae	Shrub	0.52 ± 0.01	28.5 ± 2.55	211 ± 8.26	-1.37 ± 0.07	-2.07 ± 0.11	11.5 ± 0.81	88.3 ± 0.55
Dry habitat									
C. betuloides[a]	Rosaceae	Tree	0.22 ± 0.02	8.57 ± 1.58	121 ± 23.3	-1.64 ± 0.04	-2.59 ± 0.03	10.1 ± 0.70	85.1 ± 0.80
Comarostaphylis diversifolia[a]	Ericaceae	Tree	0.49 ± 0.04	12.8 ± 0.61	253 ± 16.9	-2.51 ± 0.34	-3.45 ± 0.34	17.3 ± 2.23	85.5 ± 1.85
Hedera canariensis[a]	Araliaceae	Shrub	0.27 ± 0.02	67.2 ± 7.68	84.1 ± 11.0	-1.49 ± 0.07	-1.98 ± 0.09	12.8 ± 0.49	88.4 ± 1.40
H. arbutifolia[a]	Rosaceae	Shrub	0.38 ± 0.01	21.5 ± 2.06	185 ± 12.4	-2.08 ± 0.09	-2.53 ± 0.10	16.4 ± 0.49	87.4 ± 0.53
Q. agrifolia[a]	Fagaceae	Tree	0.30 ± 0.01	14.2 ± 0.70	188 ± 7.53	-2.31 ± 0.12	-3.00 ± 0.12	17.9 ± 1.28	87.5 ± 1.59
R. coulteri	Papaveraceae	Herb	0.36 ± 0.01	23.9 ± 0.67	78.1 ± 3.67	-1.01 ± 0.08	-1.40 ± 0.07	6.78 ± 0.33	87.2 ± 0.61
S. canariensis	Lamiaceae	Herb	0.26 ± 0.01	54.5 ± 8.28	41.4 ± 6.01	-0.92 ± 0.05	-1.18 ± 0.07	5.49 ± 0.21	83.1 ± 0.95

[a]Pressure-volume parameters are from Scoffoni et al. (2008, 2011).

leaf density (Fig. 5, D and E), as did magnitudes of $dT_{leaf}/d\Psi$, $dT_C/d\Psi$, and PLA_{dry} ($|r_p|$ and $|r_s| = 0.70$–0.87, $P < 0.05$; Supplemental Table S3). Species with thinner hydrated leaves tended to have higher PLA_{dry} (r_p and $r_s = -0.57$ to -0.62, $P < 0.05$; Supplemental Table S3). Leaf shrinkage tended to be independent of leaf area across species; only Ψ_{leaf} at 50% shrinkage in thickness showed a positive correlation with mean leaf area (r_p and $r_s = 0.55$–0.58, $P < 0.05$; Supplemental Table S3).

Leaf shrinkage was independent of most leaf vein traits. No correlation was found between $dT_{leaf}/d\Psi$ and major, minor, or total VLA (r_p and $r_s = 0.25$–0.57, $P > 0.05$; Supplemental Table S3). The few correlations observed between vein and shrinkage traits did not suggest causal dependency (Supplemental Table S3).

Cuticular conductance (g_{min}) was positively correlated with a number of leaf shrinkage parameters, such as $PLT_{leaf,TLP}$, and $PLT_{A,TLP}$, and the magnitudes of $dT_{leaf}/d\Psi$, $dT_A/d\Psi$, and PLA_{dry} ($|r_p|$ and $|r_s| = 0.65$–0.91, $P < 0.05$; Fig. 7; Supplemental Table S3).

Separating the Drivers of Leaf Shrinkage

Most leaf pressure-volume parameters and structural features that correlated with leaf shrinkage were themselves intercorrelated (Fig. 5, F–O; Supplemental Table S3). To test for effects of single traits, holding others constant, partial correlation analysis was applied to: (1) $PLT_{leaf,TLP}$, ε, and π_o; (2) $dT_{leaf}/d\Psi$, $dK_{leaf}/d\Psi$, ε, and π_o; (3) $PLT_{leaf,TLP}$, ε, and g_{min}; (4) $PLT_{leaf,TLP}$, LMA, leaf density, ε, and π_o; and (5) PLA_{dry}, g_{min}, ε, and π_o (Supplemental Table S6). These analyses enabled us to develop a model of the influences of given traits on leaf shrinkage and the hydraulic vulnerability of the xylem and outside-xylem pathways (Fig. 8). Briefly, a high major VLA provides lower xylem hydraulic vulnerability independently of leaf shrinkage, which influences the outside-xylem vulnerability. A low degree of shrinkage in thickness is achieved at the cellular level through both high ε and more negative π_o and is linked to structural traits such as LMA and leaf density through ε. The ε also controls the maximum shrinkage in leaf area, which acts directly on g_{min}.

Consistent with this model for trait influences, we found that the effects of π_o and ε on leaf shrinkage were too intercorrelated to be distinguished. Thus, when accounting for the effect of either π_o or ε, the correlation between the other trait and the $PLT_{leaf,TLP}$ disappeared ($|r_{partial}| = 0.42$–0.01, $P > 0.05$; Fig. 8; Supplemental Table S6). Similarly, LMA and leaf density were strongly related to pressure-volume parameters, and separate relationships with shrinkage could not be resolved (Figs. 5 and 8); when removing the effect of LMA or leaf density, the correlation between $PLT_{leaf,TLP}$ and pressure-volume parameters disappeared, and when removing the effect of pressure-volume parameters, the correlation of leaf shrinkage with LMA or leaf density disappeared ($|r_{partial}| = 0.06$–0.47, $P > 0.05$). However, when removing the effect of $PLT_{leaf,TLP}$, the correlation

Table III. *Symbols, terms, units, derivation, and biological significance of the nine key leaf thickness and area shrinkage traits in this study*

An additional nine traits were quantified, and their calculation and correlations with these key traits are described in Supplemental Materials and Methods S1, Supplemental Results S1, and Supplemental Tables S2 to S4.

Symbols	Parameters	Units	Derivation	Significance
Thickness shrinkage				
$PLT_{leaf,TLP}$	Percentage loss of thickness at TLP	%	From plot of PLT versus Ψ_{leaf}[a]	Estimate of leaf thickness shrinkage at TLP
$PLT_{C,TLP}$	Percentage loss of cell thickness at TLP	%	From plot of $PLT_{C,TLP}$ versus Ψ_{leaf}[a]	Estimate of the amount of cell thickness lost when cells become flaccid
$PLT_{A,TLP}$	Proportion of intercellular airspace thickness lost at TLP	%	From plot of $PLT_{A,TLP}$ versus Ψ_{leaf}[a]	Estimate of the amount of airspace thickness lost (or gained) when cells become flaccid
$dT_{leaf}/d\Psi$	Degree of shrinkage of leaf thickness	% MPa^{-1}	$\frac{PLT_{leaf,TLP}}{TLP}$	Steepness of the decline of whole-leaf thickness with Ψ_{leaf} before cells become flaccid
$dT_C/d\Psi$	Degree of shrinkage of leaf cells	% MPa^{-1}	$\frac{PLT_{C,TLP}}{TLP}$	Steepness of the decline of cell thickness with Ψ_{leaf} before cells become flaccid
$dT_A/d\Psi$	Degree of shrinkage of leaf intercellular airspace	% MPa^{-1}	$\frac{PLT_{A,TLP}}{TLP}$	Steepness of the decline of air thickness with Ψ_{leaf} before cells become flaccid
PLT_{dry}	Percentage loss of thickness in a dry leaf	%	$1 - \frac{T_{leaf,dry}}{T_{leaf,FT}}$	Maximum amount of thickness shrinkage
Area shrinkage				
$PLA_{leaf,TLP}$	Percentage loss of area at TLP	%	From plot of PLA versus Ψ_{leaf}[a]	Estimate of leaf area shrinkage at TLP
PLA_{dry}	Percentage loss of area in a dry leaf	%	$1 - \frac{A_{leaf,dry}}{A_{leaf,FT}}$	Maximum amount of area shrinkage

[a]Because thickness of the leaf or tissues precisely at TLP could not be determined, we interpolated the value for TLP by assuming a linear decline of leaf dimensions with Ψ_{leaf} between the two surrounding measurements.

between pressure-volume parameters and LMA or leaf density remained ($r_{partial} = 0.70–0.82$, $P < 0.01$).

Also consistent with our model for structural influences, we found that the linkages of leaf hydraulic vulnerability with the degree of leaf shrinkage were mediated by the pressure-volume parameters π_o and π_{TLP} (Fig. 8). Accounting for the effect of $dT_{leaf}/d\Psi$, the correlation between $dK_{leaf}/d\Psi$ and π_o or π_{TLP} disappeared ($|r_{partial}| = 0.04–0.16$, $P > 0.05$). However, the correlation between $dT_{leaf}/d\Psi$ and $dK_{leaf}/d\Psi$ remained even when accounting for the effects of π_o, π_{TLP}, or ε, and the correlations between $dT_{leaf}/d\Psi$ and π_o, π_{TLP}, and ε remained even when accounting for $dK_{leaf}/d\Psi$ ($|r_{partial}| = 0.61–0.74$, $P < 0.05$; Supplemental Table S6), indicating that the linkage of shrinkage to pressure-volume parameters was more proximal than that of hydraulic vulnerability to pressure-volume parameters.

Leaf shrinkage in thickness was apparently indirectly correlated with g_{min}. The correlation of $PLT_{leaf,TLP}$ and g_{min} seemed to be driven by their separate correlations with ε; when accounting for the effect of ε, the correlation between g_{min} and $PLT_{leaf,TLP}$ disappeared ($r_{partial} = 0.09$, $P > 0.05$; Supplemental Table S6), but ε and $PLT_{leaf,TLP}$ remained correlated after accounting for the effect of g_{min} ($r_{partial} = -0.66$, $P < 0.05$). By contrast, maximum shrinkage in area still remained tightly correlated with g_{min} after accounting for the effect of ε or π_o ($r_{partial} = 0.90–0.91$, $P < 0.001$; Fig. 8). The correlation between maximum shrinkage in area and ε or π_o was no longer significant after accounting for the strong linkage with g_{min} ($|r_{partial}| = 0.42–0.43$, $P > 0.05$; Supplemental Table S6).

Predicting Leaf Hydraulic Vulnerability from Thickness Shrinkage and Major Vein Density

Given the correlations of P_{50} and P_{80} with both major VLA and thickness shrinkage, and because according to our structural model these latter traits were related to the xylem and outside-xylem pathways, respectively, we tested whether they provided a strong prediction of P_{50} and P_{80}. Indeed, multiple regression analysis showed a greatly improved r^2 when using both thickness shrinkage and major VLA for predicting P_{50} or P_{80} ($r^2 = 0.87$ for both P_{50} and P_{80} when using both shrinkage and major VLA, versus $r^2 = 0.74–0.72$ for P_{50} or P_{80} respectively, using only major VLA and $r^2 = 0.52–0.55$ for P_{50} or P_{80} respectively, using only $dT_{leaf}/d\Psi$). The fitted models for predicting P_{50} and P_{80} were:

$$P_{50}\ predicted = 0.465 + 0.041 \times dT_{leaf}/d\Psi + 1.79 \times major\ VLA \tag{2}$$

$$P_{80}\ predicted = 1.20 + 0.070 \times dT_{leaf}/d\Psi + 2.70 \times major\ VLA \tag{3}$$

The observed P_{50} and P_{80} were strongly correlated with values predicted from these models, with the slope close to 1 (0.96–0.97) and $r^2 = 0.87$ (Fig. 9).

DISCUSSION

The results from computer modeling and experiments demonstrated that leaf shrinkage is a strong correlate

Table IV. Symbols, terms, units, derivation, and biological significance of the 28 leaf traits relating to composition, hydraulics, pressure-volume curves, water storage, and venation Δ, Change.

Symbols	Parameters	Units	Derivation	Significance
Leaf composition				
$PT_{cell,FT}$	Percentage cell thickness at full turgor	%	$\frac{T_{C,FT} \text{ or } T_{A,FT}}{T_{leaf,FT}}$	Amount of cell thickness at full hydration
$PT_{A,FT}$	Percentage air thickness at full turgor	%		Amount of air thickness at full hydration
$PT_{cell,TLP}$	Percentage cell thickness at TLP	%	$\frac{T_{C,TLP} \text{ or } T_{A,TLP}}{T_{leaf,TLP}}$	Amount of cell thickness at TLP
$PT_{A,TLP}$	Percentage air thickness at TLP	%		Amount of air thickness at TLP
LMA	Leaf mass per area	g m^{-2}	Leaf dry mass per leaf area	—
Leaf density	—	g cm^{-3}	Leaf dry mass per leaf volume	—
FA	Fraction air	—	(Leaf mass after water infiltration of the airspaces − leaf turgid mass) / leaf volume	Estimate of the amount of airspace in the leaf
FW	Fraction water	—	(Leaf turgid mass − leaf dry mass) / leaf volume	Estimate of the amount of water in the leaf
FS	Fraction solid	—	1 − fraction air − fraction water	Estimate of the amount of solid in the leaf
Percentage air in a dry leaf	—	%	Leaf dry thickness × (1 − fraction solid in dry leaf)	Estimate of the amount of airspace in a dry leaf
Leaf hydraulics				
K_{max}	Maximum leaf hydraulic conductance	mmol m^{-2} s^{-1} MPa^{-1}	y intercept of the maximum likelihood function of the vulnerability curve	Efficiency of water movement through a fully hydrated leaf
K_{TLP}	Leaf hydraulic conductance at TLP	mmol m^{-2} s^{-1} MPa^{-1}	Parameter of fitted vulnerability curve	Efficiency of water movement at π_{TLP}
P_{50}	Ψ_{leaf} at 50% loss of K_{leaf}	MPa	Parameter of fitted vulnerability curve	—
P_{80}	Ψ_{leaf} at 80% loss of K_{leaf}	MPa	Parameter of fitted vulnerability curve	—
$dK_{leaf}/d\Psi$	Slope of the leaf hydraulic vulnerability curve at $\Psi_{leaf} = -0.5$ MPa	mmol m^{-2} s^{-1} MPa^{-1}	Parameter of fitted vulnerability curve	Vulnerability of K_{leaf} to dehydration
g_{min}	Cuticular conductance	mmol m^{-2} s^{-1}	Directly measured	Minimal epidermal conductance after stomatal closure
Pressure-volume curve parameters				
$\pi_{TLP} = TLP$	Osmotic pressure at TLP	MPa	Parameter of pressure-volume curve	Water potential at which cells become flaccid
π_o	Osmotic pressure at full turgor	MPa	Parameter of pressure-volume curve	Concentration of solutes in cells
ε	Modulus of elasticity	MPa	Parameter of pressure-volume curve	Wall stiffness, i.e. Δ turgor pressure/ Δ RWC
RWC_{TLP}	Relative water content at TLP	%	Parameter of pressure-volume curve	Leaf hydration when cells become flaccid
Water storage				
C_{FT}	Capacitance at full turgor	MPa^{-1}	$\Delta(100 - RWC)/\Delta \Psi_{leaf}$ before π_{TLP}	Amount of water storage before π_{TLP}
C_{TLP}	Capacitance at TLP	MPa^{-1}	$\Delta(100 - RWC)/\Delta \Psi_{leaf}$ past π_{TLP}	Amount of water storage after π_{TLP}
SWC	Saturated water content	g g^{-1}	Fresh mass − dry mass/leaf dry mass	Water storage index
C^*_{FT}	Leaf area-specific C_{FT}	mol m^{-2} MPa^{-1}	$C_{FT} \times SWC \times LMA$	—
C^*_{TLP}	Leaf area-specific C_{TLP}	mol m^{-2} MPa^{-1}	$C_{TLP} \times SWC \times LMA \times RWC_{TLP}$	—
Leaf venation				
Major VLA	Major vein length per area	mm mm^{-2}	Major vein length/leaf area	Sum of first, second, and third order vein lengths per leaf area
Minor VLA	Minor vein length per area	mm mm^{-2}	Minor vein length/leaf area	Sum of fourth and higher order vein lengths per leaf area
VLA	Vein length per area	mm mm^{-2}	Vein length/leaf area	Sum of major and minor vein lengths per leaf area
Ratio major to minor	Ratio of major to minor VLA	—	Major VLA/minor VLA	Leaf venation composition index
FEV	Free-ending veins per area	No. mm^{-2}	No. of free-ending veins per area	—

Table V. *Percentage loss of thicknesses and area at TLP and for oven-dried leaves*
nd, Not determined; ***, $P < 0.001$.

Species	$PLT_{leaf,TLP}$	PLT_{dry}	$PLT_{C,TLP}$	$PLT_{A,TLP}$	$PLA_{leaf,TLP}$	PLA_{dry}
B. galpinii	16 ± 2.3	83 ± 1.5	19 ± 0.31	14 ± 5.1	0.48 ± 0.16	21 ± 0.94
C. sasanqua	15 ± 1.2	43 ± 1.1	21 ± 0.30	3.3 ± 5.2	2.9 ± 0.38	5.0 ± 2.2
C. betuloides	18 ± 3.6	33 ± 5.0	11 ± 1.2	39 ± 16	4.8 ± 0.51	21 ± 2.3
C. diversifolia	12 ± 1.4	44 ± 1.9	16 ± 0.32	6.8 ± 3.4	1.2 ± 0.79	10 ± 0.88
H. canariensis	11 ± 1.3	62 ± 3.8	11 ± 0.18	−5.9 ± 8.7	0.96 ± 0.25	16 ± 0.93
Sunflower	22 ± 1.2	36 ± 1.6	nd	nd	14 ± 0.62	69 ± 1.4
H. arbutifolia	12 ± 2.1	53 ± 1.1	14 ± 0.51	7.8 ± 6.5	0.74 ± 0.27	4.9 ± 2.0
L. camara	38 ± 2.0	80 ± 1.9	16 ± 0.54	77 ± 5.3	9.4 ± 0.43	45 ± 2.1
M. grandiflora	22 ± 1.8	42 ± 3.3	11 ± 0.52	30 ± 1.9	nd	8.2 ± 1.1
P. racemosa	36 ± 4.0	70 ± 2.7	12 ± 0.48	72 ± 0.0	1.3 ± 0.47	26 ± 2.1
Q. agrifolia	5.1 ± 0.92	23 ± 1.7	15 ± 0.15	−12 ± 3.4	1.6 ± 0.13	7.0 ± 0.14
R. indica	4.6 ± 0.38	47 ± 2.2	12 ± 0.14	−1.8 ± 4.9	0.61 ± 0.31	14 ± 0.45
R. coulteri	16 ± 1.6	50 ± 1.5	12 ± 0.29	25 ± 5.3	3.9 ± 0.28	28 ± 1.4
S. canariensis	28 ± 7.2	66 ± 1.5	nd	nd	8.4 ± 1.1	57 ± 2.7
One-way ANOVA	***	***	***	***	***	***

and potential driver of leaf hydraulic vulnerability along with other drivers, such as xylem embolism and collapse, and aquaporin deactivation. Our detailed examination of leaf shrinkage provides new insight into its mechanisms and variation across species. Moreover, our results have strong ecological implications, given the great variation in shrinkage across species, with species native to dry habitat more resistant to shrinkage due to their more negative π_o or π_{TLP} (Ψ_{leaf} at TLP) and higher ε.

Impact of the Mesophyll on Leaf Hydraulic Vulnerability: Insights from the Computer Model

Results from model simulations confirmed the hypothesis that decline in extraxylem conductance should have strong impacts on K_{leaf} vulnerability, especially at high Ψ_{leaf}. The initial slope of K_{leaf} against Ψ_{leaf} was nearly as steep when only the extraxylem component was vulnerable to hydraulic decline as when both xylem and extraxylem components were vulnerable. Similarly, the impact of extraxylem vulnerability on the Ψ_{leaf} at P_{50} and P_{80} pointed to its particular influence on the early decline of K_{leaf}. The model simulations were consistent with a more vulnerable extraxylem component protecting the xylem from tensions that would cause embolisms and strong stomatal closure. Along the hydraulic pathway, the tension generated by transpiration is dissipated by frictional losses proportional to hydraulic resistance. As expected, simulations showed that in leaves where $R_{ox} > R_x$, and thus the extraxylem bottleneck was more pronounced, negative pressures would build up less strongly in the xylem for a given bulk Ψ_{leaf} than if $R_x > R_{ox}$. Substantial extraxylem resistance protects the xylem water pressure from declining to values that would trigger air seeding, thus leading to the S-shaped curve seen in the simulation where only the xylem is vulnerable (Fig. 2A, light gray dashed line). Additionally, an $R_{ox} > R_x$ scenario allows cavitation to occur at more negative Ψ_{leaf} than if $R_x > R_{ox}$ (Table I). Furthermore, regardless of the relative values of R_{ox} and R_x in the

turgid leaf, extraxylem vulnerability always had a strong impact on the decline of K_{leaf} at high Ψ_{leaf} (Fig. 2, gray dashed lines). We note that this model assumed a steady-state transpiration rate. Short-term dynamics of mesophyll water potential could act directly on stomatal aperture and thus feedback on stomatal conductance and transpiration, but the principles shown here would act when steady state was established.

These model results are analogous to the hydraulic segmentation theory proposed for whole-tree architecture (Zimmermann, 1978). According to that theory, high resistances are found in the most distal parts of the trees (leaves, then lateral branches), so that tensions will be disproportionately large there, and reduced in proximal parts, thus delaying the onset of embolisms in the main
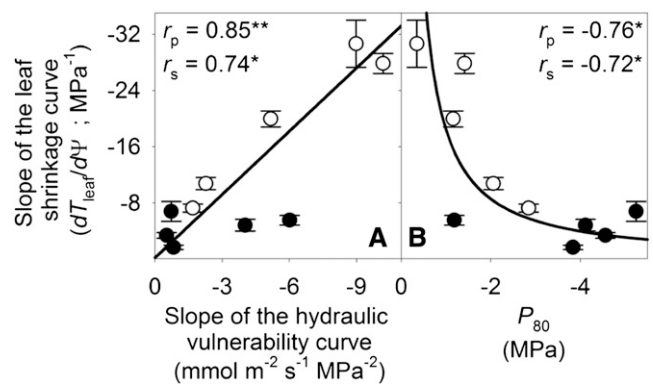

Figure 4. Coordination of leaf shrinkage and leaf hydraulic vulnerability in 10 species of diverse leaf form and texture and drought tolerance. The slope of leaf hydraulic vulnerability at $\Psi_{leaf} = -0.5$ MPa (A) and Ψ_{leaf} at 80% loss of hydraulic conductance (B) were plotted against slope of total leaf thickness shrinkage before TLP. Species from moist habitats are represented in white, and woody species from dry habitats are represented in black. Fitted standardized major axes are as follows: $dT_{leaf}/d\Psi = 3.0 \times dK_{leaf}/d\Psi - 0.22$ for A and $dT_{leaf}/d\Psi = 18 \times P_{80}^{-1.1}$ for B. *$P < 0.05$, **$P < 0.01$.
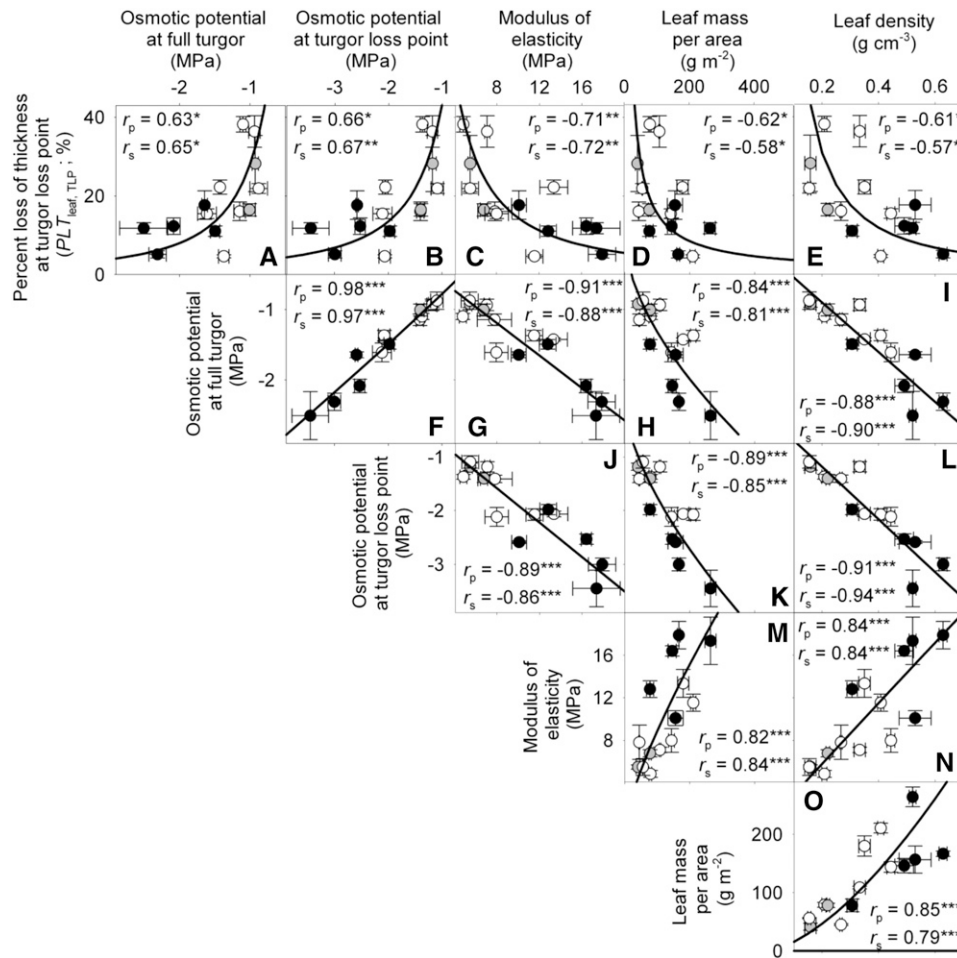
Figure 5. Relationship of loss of leaf thickness at TLP with pressure-volume curve parameters and leaf structural traits for 14 species of diverse leaf form and texture and drought tolerance. A to E show traits plotted against the percentage loss of leaf thickness at TLP: leaf osmotic potential at full turgor (A), leaf osmotic potential at TLP (B), ε (C), LMA (D), and leaf density (E). F to O show the intercorrelation of those five traits. Species native to moist habitats are represented in white, woody species from dry habitats are represented in black, and herbs from dry habitats are represented in gray. Fitted standardized major axes are as follows: $PLT_{leaf,TLP} = -28 \times \pi_o^{-1.8}$ for A, $PLT_{leaf,TLP} = -44 \times \pi_{tlp}^{-1.7}$ for B, $PLT_{leaf,TLP} = 357 \times \varepsilon^{-1.4}$ for C, $PLT_{leaf,TLP} = 906 \times LMA^{-0.88}$ for D, $PLT_{leaf,TLP} = 3.3 \times Leaf\ density^{-1.4}$ for E, $\pi_o = -0.78 \times \pi_{tlp}^{-0.93}$ for F, $\pi_o = -0.11 \times \varepsilon - 0.27$ for G, $\pi_o = -0.09 \times LMA^{-0.59}$ for H, $\pi_o = -3.5 \times Leaf\ density - 0.20$ for I, $\pi_{tlp} = -0.16 \times \varepsilon - 0.31$ for J, $_{tlp} = -0.09 \times LMA^{-0.64}$ for K, $\pi_{tlp} = -4.9 \times Leaf\ density - 0.20$ for L, $\varepsilon = 0.25 \times LMA^{0.77}$ for M, $\varepsilon = 28 \times Leaf\ density^{0.99}$ for N, and $LMA = 581 \times Leaf\ density^{1.6}$ for O. *$P < 0.05$, **$P < 0.01$, ***$P < 0.001$.

trunk xylem, crucial for the tree's survival. We found that resistance in the extraxylem component and its increase during leaf dehydration would prevent stronger tensions in the leaf vein xylem and delay the onset of xylem embolism or collapse. In essence, vulnerability in the xylem and extraxylem pathways partitions the low water potential caused by a given transpiration rate; greater vulnerability in extraxylem pathways preferentially partitions low potentials to the mesophyll, possibly delaying xylem embolism and strong stomatal closure.

Thus, in sum, decline in the extraxylem conductivity, which would likely occur during leaf shrinkage, leads to strong K_{leaf} reductions and protects the xylem from embolism during ongoing transpiration, which would lead to yet stronger K_{leaf} reductions and potentially

necessitate energy for refilling xylem conduits (Nardini et al., 2011).

Impact of Leaf Shrinkage on Leaf Hydraulic Vulnerability

Previous studies showed that K_{leaf} decline in dehydrating leaves was correlated not only with xylem embolism but also with biochemical processes outside the xylem, such as aquaporin deactivation (Johansson et al., 1998; Kim and Steudle, 2007; Scoffoni et al., 2012). To our knowledge, our study is the first to implicate a physical influence of leaf shrinkage in the decline of K_{leaf} with dehydration, using the same correlational approach. These results support our model findings that extraxylem
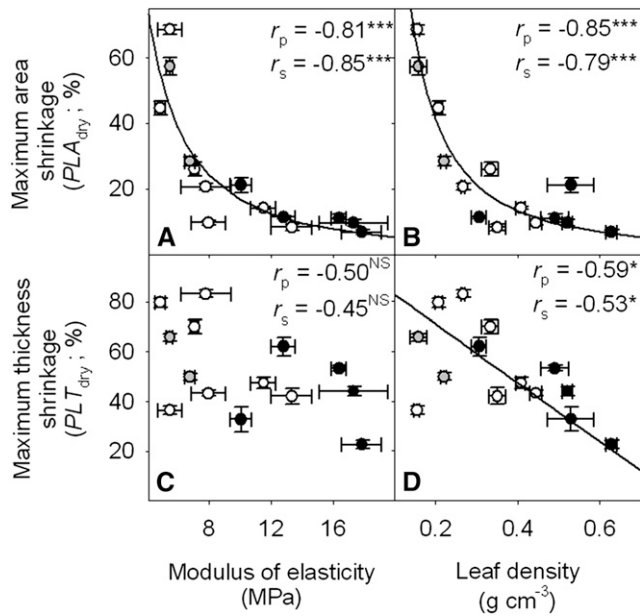
Figure 6. Coordination of maximum leaf area and thickness shrinkage with ε and leaf density for 14 species of diverse leaf form and texture and drought tolerance. A, $PLA_{dry} = 757 \times \varepsilon^{-1.7}$. B, $PLA_{dry} = 2.96 \times Leaf\ density^{-1.6}$. C, $PLT_{dry} = -118 \times Leaf\ density + 94.7$. $^{NS}P > 0.05$, $*P < 0.05$, $***P < 0.001$. (Symbols as in Fig. 5.)

hydraulic decline would in principle impact on K_{leaf} for a given species. Furthermore, consistent with our hypotheses and the results of the model simulations, our experiments using diverse species confirmed the hypothesis that K_{leaf} declines were correlated across species with leaf thickness shrinkage, especially at high Ψ_{leaf}. Species that experienced the most severe shrinkage above TLP had steeper initial K_{leaf} declines and less negative P_{80} values.

Is there an adaptive hydraulic function for a species' greater thickness shrinkage? As for our modeled results, a mechanism was suggested by the segmentation theory of Zimmermann (1978). Thickness shrinkage reduces K_{leaf} when the mesophyll, but not yet the xylem itself, experiences very negative water potential; this would amplify any water status signal that causes stomatal closure, thus preventing further decline in Ψ_{leaf} and sparing the xylem from embolism. Thus, species with xylem especially sensitive to air seeding would benefit from shrinkage that would reduce the conductance outside the xylem. Such "sacrifice" of mesophyll hydraulic conductance during dehydration would also be expected to delay intense cavitation during daily transpiration. This mechanism would be particularly useful given the partial reversibility of even strong leaf shrinkage shown by our rehydration experiments. After 1 h of rehydration, leaf discs had regained more than half their initial thickness, regardless of their level of dehydration (Supplemental Results S3; Supplemental Discussion S1).

Indeed, although shrinkage has not been previously investigated in this way, previous studies have pointed

to a role of extraxylem pathways in K_{leaf} decline (for review, see Scoffoni et al., 2012). Recent studies of Arabidopsis suggested that bundle sheath cells acted as valves during drought by converting chemical signals from the vein xylem, such as abscisic acid, into a decrease in K_{leaf} by deactivating aquaporins (Shatil-Cohen et al., 2011; Pantin et al., 2012). Our modeling and experimental work were consistent in implicating reductions in the extraxylem pathways, whether caused by aquaporin deactivation, cell shrinkage, or both, in the decline of K_{leaf} with dehydration. Future work is needed to fully resolve the roles of xylem and extraxylem pathways and their interaction in determining the response of K_{leaf} to dehydration.

Drivers of Leaf Shrinkage and Its Relation to Leaf Vulnerability

Our experiments provided insight into processes occurring within specific leaf tissues during shrinkage (Supplemental Discussion S2). What are the structural factors that influence leaf shrinkage and thus hydraulic vulnerability? Previous studies have reported a correlation of hydraulic vulnerability with the pressure-volume parameters π_o and π_{TLP} (Crombie et al., 1985; Blackman et al., 2010; Scoffoni et al., 2012). This linkage could arise because a more negative π_{TLP} enables cells to maintain structural integrity (i.e. a higher RWC at lower Ψ_{leaf}; Blackman et al., 2010; Scoffoni et al., 2012). That hypothesis was supported in our study: the $PLT_{leaf,TLP}$ was lower in species with more negative π_o and higher ε. Our findings for the linkage of shrinkage with pressure-volume parameters confirmed and expanded those of studies of fewer species. In one study of six species, leaves of woody plants shrank less than those of herbs,
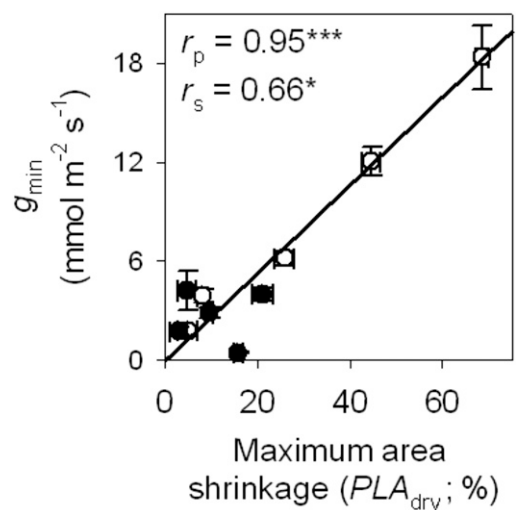

Figure 7. Relationship between g_{min} and maximum leaf area shrinkage for 14 species of diverse leaf form and texture and drought tolerance. $g_{min} = 0.27 \times PLA_{dry} - 0.08$. $*P < 0.05$, $***P < 0.001$. (Symbols as in Fig. 4.)
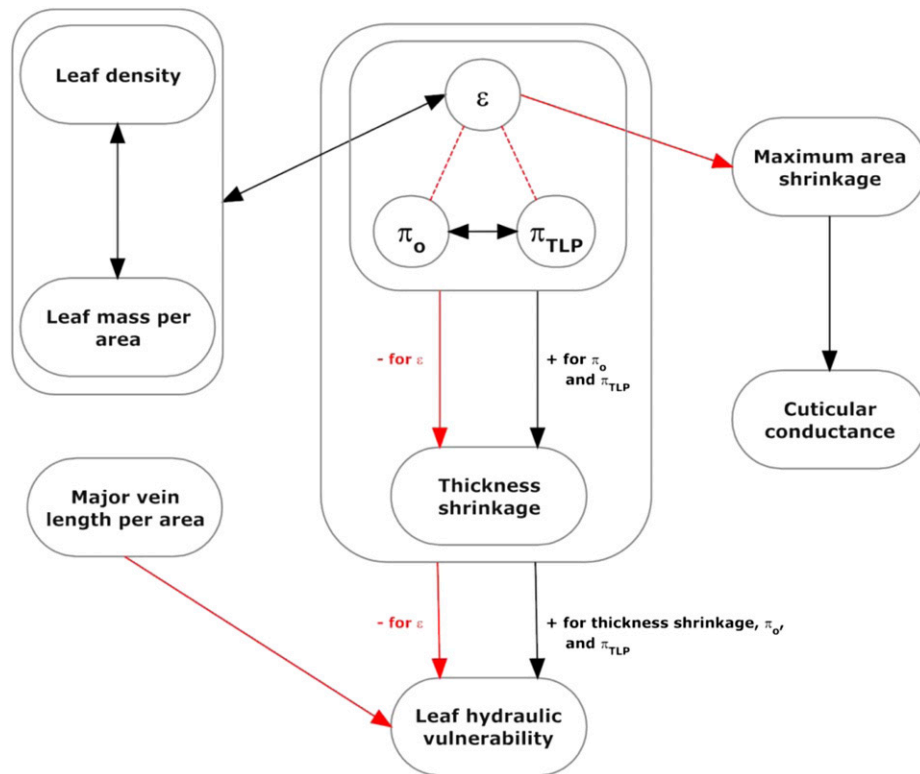
Figure 8. Synthetic conceptual hypothesis for trait associations and impacts of leaf shrinkage and structural traits on leaf hydraulic vulnerability. Leaf hydraulic vulnerability is influenced independently by major VLA acting on the xylem pathways and leaf shrinkage in thickness acting on the outside-xylem pathways of water movement through the leaf. Thickness shrinkage is determined by cell properties (i.e. the pressure-volume curves parameter ε, π_o, and π_{TLP}). The dotted lines signify that the ε and osmotic pressures are not directly linked but strongly associated; saltier cells need a higher ε to maintain RWC at TLP above lethal levels (Bartlett et al., 2012b). The ε, being related to cell wall thickness, is correlated with leaf density and LMA, which are also related to cell wall thickness; thus, all these variables influence thickness shrinkage. The ε also influences PLA_{dry}. PLA_{dry} and not ε acts directly on g_{min}, possibly through enhanced leaky stomata (see Supplemental Discussion S2). Red arrows indicate significant negative correlations between traits, while black arrows indicate significant positive correlations between traits. Double-headed arrows indicate traits that are too intrinsically linked to tease apart. [See online article for color version of this figure.]

potentially due to their more negative π_o (Kennedy and Booth, 1958). In another study, species with low ε shrank more strongly in thickness (Syvertsen and Levy, 1982). In our study, partial correlation analysis could not tease apart the effects of π_o and ε on $PLT_{leaf,TLP}$, due to their strong association, and their combined impacts on determining cell shrinkage at TLP and thus RWC at TLP (Bartlett et al., 2012b). These results support the hypothesis that cell shrinkage depends on cell structural integrity (i.e. the pressure-volume parameters) and shrinkage influences leaf hydraulic vulnerability.

Tissue shrinkage may affect K_{leaf} decline by altering the pathways for water movement. The precise pathways of mesophyll water movement and, indeed, the identity of the cells that are the sites of water evaporation have remained puzzling questions for decades (Meidner, 1983). Three main pathways for water movement outside the xylem have been proposed: (1) water flows from the xylem to the bundle sheath cells and principally evaporates there (Boyer, 1985); (2) water flows mainly through or around epidermal cells, which

have their walls better interconnected than mesophyll and palisade cells, and evaporates near stomata (Wylie, 1943; Sheriff and Meidner, 1974; Meidner, 1975); and (3) water evaporates from the mesophyll cells, but an appreciable part evaporates as well from the epidermal cells (Farquhar and Raschke, 1978). Cell shrinkage can reduce connections for water to flow (Sancho-Knapik et al., 2011) and additionally would reduce evaporative surface; both effects would reduce K_{leaf}. Tissue shrinkage during transpiration might in fact highlight where water principally evaporates within the leaf and how it varies among species (Canny et al., 2012). While *Eucalyptus* species showed equal shrinkage throughout the mesophyll, suggesting that transpirational water evaporates throughout the leaf, cotton (*Gossypium hirsutum*) showed the strongest shrinkage and potentially greater evaporation in the spongy mesophyll and in palisade cells surrounding the substomatal cavities (Canny et al., 2012). Whether the shrinkage of given leaf tissues or populations of cells has more effect than others on K_{leaf} (e.g. bundle sheath cells; Scoffoni et al., 2012)
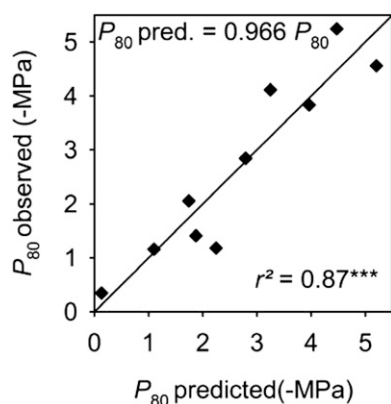
Figure 9. Ability of a model to predict P_{80} from an equation based on leaf shrinkage and major VLA (Eq. 3). The plot of observed versus predicted values, with line fitted through the origin, showed low bias (slope close to 1.0) and very high r^2. Similar predictive power was found for P_{50} (see "Results"). ***$P < 0.001$.

remains to be elucidated. Furthermore, it is unknown whether K_{leaf} decline is due to the direct effect of the physical impact of leaf shrinkage on hydraulic pathways, to an indirect effect of cell shrinkage on aquaporin activity (Johansson et al., 1998; Kim and Steudle, 2007), or to both. The shrinkage of airspaces may reflect structural changes (i.e. cell wall buckling) that would reduce extraxylem water flow by reducing cell contact and/or the conductance of cell walls.

The strength of the correlation of K_{leaf} vulnerability with leaf shrinkage, together with the model simulation results and the clear physical linkage of the pathways of water movement with cellular structure and tissue integrity, support a mechanistic linkage between vulnerability and shrinkage. An alternative argument, that the linkage of K_{leaf} vulnerability with leaf shrinkage is only circumstantial (i.e. that these responses are independently linked across species due to their association with moist habitat) remains possible. However, it is common to use physical principles to postulate a mechanistic basis for correlations. For example, this was used to establish connections between maximum K_{leaf} and leaf hydraulic vulnerability with xylem structure (i.e. with midrib conduit dimensions and VLA; Sack and Frole, 2006; Brodribb et al., 2007; Blackman et al., 2010; Scoffoni et al., 2011; Nardini et al., 2012), and here we have extended this approach to the extraxylem pathways. Further validation of this hypothesis will require tests using mutant phenotypes in model species and/or mechanistic manipulations to establish absolute causality.

Coupling the Effects of Leaf Shrinkage and Leaf Veins to Better Predict Hydraulic Vulnerability

Previous researchers hypothesized that leaf veins act as a "skeleton" that reduces leaf shrinkage during dehydration (Gardner and Ehlig, 1965). We found no

relationship across species of the degree of shrinkage with major or total VLA. Instead, we found shrinkage to be closely related to leaf properties principally determined by mesophyll cells, π_o and ε. Notably, in some species, bundle sheath extensions (especially when fibrous) could play an important role in reducing shrinkage (Cutler, 2005; Pivovaroff et al., 2014).

Previous work showed that a greater major VLA reduces the leaf hydraulic vulnerability, providing more pathways for the water to flow around embolisms (Scoffoni et al., 2011). Thus, leaf shrinkage and the venation architecture are independent factors that both influence the vulnerability of K_{leaf}, factors representing the xylem and outside-xylem components, respectively. We found that including both major VLA and shrinkage led to a stronger ability to predict P_{50} and P_{80} than either factor alone, and Equations 2 and 3 provided a very strong prediction (Fig. 9), the strongest to our knowledge of leaf hydraulic vulnerability based on structural measurements. Previous work has also shown that P_{50} and/or P_{80} can be predicted across species by the dimensions of minor vein xylem conduits (Blackman et al., 2010) and that hydraulic decline of K_{leaf} and/or cell permeability can be related to properties of aquaporins and the effects of abscisic acid (Kim and Steudle, 2007; Shatil-Cohen et al., 2011). Our Equations 2 and 3 should be validated and extended with measurements for additional species, as they point to a great potential for estimating hydraulic vulnerability from easily measurable traits.

Applications of Leaf Shrinkage for Drought Monitoring and Drought Tolerance Assessment

Our findings support previous studies showing the uses of shrinkage for monitoring drought responses (i.e. for estimating RWC or Ψ_{leaf} from leaf thickness and area for given leaves; Meidner, 1952; Jones, 1973; Tyree and Cameron, 1977). Our study further points to the importance of resistance to shrinkage as a trait contributing to drought tolerance (Supplemental Discussion S3). Leaf shrinkage may have novel applications for the rapid estimation of drought tolerance parameters. In addition to the ability of shrinkage to predict K_{leaf} vulnerability described above, the very strong relationship between PLA_{dry} and ε highlights the potential for the estimation of ε using Equation 1 and easy, rapid measurements of PLA_{dry}. This equation should be validated and extended for additional species, for rapid estimation of ε, which typically is obtained from pressure-volume curves, and can take 1 to 2 d of measurements per species. Such rapid measurement of a key pressure-volume parameter complements the recently described osmometer measurement of π_o and π_{TLP} (Bartlett et al., 2012a).

Because species from drier habitats experienced less shrinkage in thickness, PLT_{dry} may be a good proxy trait for evaluating drought tolerance rapidly. By contrast, PLA_{dry} may be of limited value as a drought tolerance predictor, although a good proxy for ε. Notably, ε is not a general predictor of drought tolerance, although

it may contribute to the tolerance of incipient drought by preventing early K_{leaf} decline and/or contribute indirectly to drought tolerance by preventing cell shrinkage to lethal levels. Indeed, a recent study quantified PLA_{dry} in 380 diverse species (Blonder et al., 2012) and found PLA_{dry} to be slightly higher for dry habitat species, although that trend may have arisen due to error in the measurements. In that study, PLA_{dry} was determined without first rehydrating the leaves to full turgidity, and erroneous negative PLA_{dry} data were included in that study. Such errors need to be avoided for accurate species comparisons, especially if values are to be used as proxies for more intensive physiological or ecological parameters.

CONCLUSION

Leaf shrinkage was tightly correlated with hydraulic responses, leaf and cell structure and composition, and drought adaptation. Consequently, leaf shrinkage parameters can be used as proxies for estimating hydraulic vulnerability, ε, and potentially drought adaptation. Future research on the anatomical basis of shrinkage, the precise mechanisms of leaf hydraulic decline, and the role of shrinkage-related traits in drought tolerance for a wide range of species can capitalize on these discoveries and improve the full range of their applications.

MATERIALS AND METHODS

Computer Modeling of the Theoretical Importance of the Xylem and Extraxylem Water Transport Pathways for Leaf Hydraulic Vulnerability

To refine our hypothesis that leaf shrinkage should influence leaf hydraulic vulnerability, we improved the K_leaf program (written by Hervé Cochard; Cochard et al., 2004b; McKown et al., 2010; Scoffoni et al., 2011; available on request from herve.cochard@clermont.inra.fr) to generate leaf hydraulic vulnerability curves. K_leaf creates a spatially explicit model of a leaf with up to six vein orders represented as a square grid of xylem resistors with outside-xylem resistors ("mesophyll" resistors) branching orthogonally from each junction of the vein grid. In modeled leaves, water exits through the mesophyll resistor located at each vein junction, with the bulk of the water exiting from the junctions of the minor veins. The model determines the hydraulic conductances of the xylem and outside-xylem pathways and of the whole leaf for leaves simulated with a given leaf size, length, and cross-sectional conductivity of each vein order and mesophyll hydraulic conductance. K_leaf 6.1 (developed for this study from the previous version 6.0) can simulate the loss of hydraulic conductance in each vein order and the mesophyll, corresponding to the effects of embolism and shrinkage, according to a typical vulnerability curve (Pammenter and Vander Willigen, 1998):

$$\text{PLC}_i = 100 / \left(1 + e^{(s/25) \times (P_x - P_{50})} \right) \tag{4}$$

where PLC_i is the percentage loss of hydraulic conductance in a given vein order or in the mesophyll, P_x is the pressure at that specific location, and s is the slope of the vulnerability curve. Having specified these component PLC responses, one can use K_leaf 6.1 to generate leaf hydraulic vulnerability curves (i.e. K_{leaf} versus Ψ_{leaf}) by imposing different transpiration rates, obtaining leaves with a range of different Ψ_{leaf} values corresponding to different tensions across vein orders and mesophyll. Simulations were run using a realistic elliptical leaf with an area of 9.1 cm^2, with 12 pairs of second-order veins and a total VLA of 6.9 mm mm^{-2}, and maximum vein cross-sectional conductivities based on estimations from measured xylem conduit dimensions

in *Juglans regia* (as described by Scoffoni et al. [2011]). The findings would be applicable to other leaves with hierarchical reticulate venation (McKown et al., 2010).

We ran four types of simulations to test the relative impacts of differences in vulnerability between the vein xylem and extraxylem mesophyll. (1) All the vein orders and the mesophyll were assigned the same vulnerability, with P_{50} of -1 MPa. (2) All the vein orders were assigned the same vulnerability, with P_{50} of -1 MPa, while the mesophyll was assigned greater vulnerability, with P_{50} of -0.25 MPa. (3) All the vein orders were assigned the same vulnerability, with P_{50} of -0.25 MPa, while the mesophyll was assigned lower vulnerability, with P_{50} of -1 MPa. (4) All the vein orders and the mesophyll were assigned the same vulnerability, with P_{50} of -0.25 MPa. We used the slope parameter of 200 MPa^{-1} in Equation 1 for all simulations, which is in the range of previously reported values (Pammenter and Vander Willigen, 1998). Because species also vary in the proportion of resistance distributed between xylem and outside-xylem pathways even when leaves are well hydrated (Sack et al., 2004, 2005), we ran each of the four simulations with two different parameterizations: (1) for well-hydrated leaves, most hydraulic resistance was outside the xylem (R_{ox} = 71%–76% of leaf resistance); or (2) for well-hydrated leaves, most resistance was inside the xylem (R_{ox} = 36%–42% of leaf resistance). To achieve these two types of leaves, we modified the conductivities of the first and second vein orders and the mesophyll (because of their high impacts on hydraulic conductances of the xylem and outside-xylem pathways, respectively), such that the K_{leaf} at full hydration had a similar value (7.54–8.95 mmol m^{-2} s^{-1} MPa^{-1}).

For each simulation, we constructed vulnerability curves by plotting K_{leaf} against Ψ_{leaf}, which was considered as equivalent to the modeled apoplastic mesophyll pressure. We fitted five types of functions to the curves, as used previously in the literature (Pammenter and Vander Willigen, 1998; Scoffoni et al., 2012), selecting the maximum likelihood model using the optim function in R 2.9.2 (http://www.r-project.org; Burnham and Anderson, 2002, 2004; Sack et al., 2006): linear ($K_{leaf} = a\Psi_{leaf} + y_0$), two-parameter sigmoidal $\left(K_{leaf} = \frac{100}{1 + e^{(a(\Psi_{leaf} - b))}} \right)$ (Pammenter and Vander Willigen, 1998), three-parameter sigmoidal $\left(K_{leaf} = \frac{a}{1 + e^{-\left(\frac{\Psi_{leaf} - x_0}{b}\right)}} \right)$, logistic $\left(K_{leaf} = \frac{a}{1 + \left(\frac{\Psi_{leaf}}{x_0}\right)^b} \right)$, and exponential ($K_{leaf} = y_0 + ae^{-b\Psi_{leaf}}$). From the maximum likelihood function for each simulated whole-leaf vulnerability curve, we estimated the K_{leaf} at $\Psi_{leaf} = 0$ MPa (K_{max}), the Ψ_{leaf} at which $K_{leaf} = 0.5 K_{max}$ and $0.20 K_{max}$ (P_{50} and P_{80}, respectively), and the initial slope of the vulnerability curve at $\Psi_{leaf} = -0.1$ MPa.

Experimental Plant Material

Leaf shrinkage and its relationship to other physiological traits were determined for 14 species from 12 plant families selected for diversity in leaf size, shape, and drought tolerance. Species were sampled within and around the campus of the University of California, Los Angeles, and Will Rogers State Park, in Los Angeles, from November 2009 to May 2011 (Table II). Leaves from sunflower (*Helianthus annuus* var Sunspot; Botanical Interests) were collected from greenhouse plants grown from seeds in 3.6-L pots (average minimum, mean, and maximum values for temperature, 21.1°C, 23.2°C, and 26.0°C; for humidity, 44%, 51%, and 59%). Sunflowers were irrigated every 2 d, with 200 to 250 ppm solution of 20:20:20 nitrogen:phosphorus:potassium; the photosynthetically active radiation measured at midday on a sunny day was up to 550 μmol photons m^{-2} s^{-1} and, on average, 300 μmol photons m^{-2} s^{-1} (LI-250 light meter; LI-COR Biosciences).

Shoots with mature leaves were collected from the sun-exposed part of three individuals of each species (the entire stem for sunflowers) and then recut and rehydrated overnight in ultrapure water (0.22-mm Thornton 200 CR; Millipore).

Leaf Shrinkage Experiments: Testing Leaf Responses to Dehydration

Leaf shrinkage experiments were conducted on leaves detached from the rehydrated shoots of each species ($n = 5$ leaves per species) and placed in sealed bags (Whirl-Pak; Nasco) that had previously been exhaled in to prevent water loss. The parameters of shrinkage and hydraulics measured for excised leaves were assumed to be representative of those for leaves dehydrating on the plant (Supplemental Materials and Methods S1).

To quantify leaf shrinkage, each leaf was measured for area, thickness, mass, and volume at full hydration and during progressive dehydration (for additional details, see Supplemental Materials and Methods S1). Leaves were taped by their petioles to a metal bar in front of a fan to dehydrate and repeatedly

removed for measurement. Leaf area was measured using a flatbed scanner (Canon Scan Lide 90; Canon) followed by image analysis (ImageJ software version 1.42q; National Institutes of Health). Leaf thickness was determined by averaging values taken in the centers of the bottom, middle, and top thirds of the leaf, using digital calipers (±0.01 mm; Fowler). Leaf mass was determined using an analytical balance (±0.01 mg; XS205; Mettler). Volume was determined as the product of leaf thickness and area. Once leaves had dehydrated beyond TLP or became too brittle to handle, they were placed in an oven for at least 3 d at 70°C before the dry leaf area, thickness, and mass were determined.

We partitioned the leaf thickness (i.e. the volume per area) into that of the cells and airspace (Roderick et al., 1999). The "thickness" of the cells ($T_{C,i}$) and of intercellular airspace ($T_{A,i}$) at each level i of dehydration were calculated:

$$T_{C,i} = \frac{\nu_{water,i}}{LA_i} \quad (5)$$

$$T_{A,i} = T_i - T_{C,i} \quad (6)$$

where ν_i is the volume of water at level i of dehydration (i.e. fresh leaf mass minus dry mass, divided by 1.0 g cm^{-3}) and LA_i and T_i are the leaf area and thickness at dehydration level i. In this calculation, we assumed, based on observations of anatomical cross-sections (John et al., 2013), that the volume of the protoplasts and airspace would each be much greater than that of the solid component of the cell wall. In our calculation, the volume of cell walls would be counted with that of the airspace. However, our calculation of shrinkage parameters involved changes in the dimensions of each component with changes in leaf water status, and these parameters would not be affected by the volume of the cell wall, which would be effectively unchanged during leaf dehydration.

To plot leaf shrinkage responses for leaf area, the thickness of the leaf, cells, and airspace, and leaf volume, we calculated the absolute percentage loss at a given level of dehydration:

$$PLX_i(\%) = \left(1 - \frac{X_i}{X_{FT}}\right) \times 100 \quad (7)$$

where X_i, and X_{FT} represent the leaf area, leaf thickness, leaf cell thickness, leaf airspace thickness, and leaf volume at dehydration level i and for a fully turgid leaf, respectively.

The RWC (unitless) in the leaf at each dehydration level i was calculated as:

$$RWC_i = \frac{m_{leaf,i} - m_{leaf,dry}}{m_{leaf,FT} - m_{leaf,dry}} \quad (8)$$

where $m_{leaf,i}$ is the mass of the leaf at dehydration level i, $m_{leaf,FT}$ is the mass of the leaf at full hydration, and $m_{leaf,dry}$ is the mass of the dry leaf (in g).

Leaf Shrinkage Experiments: Estimation of Ψ_{leaf} for Dehydrating Leaves

For high resolution of the shrinkage responses of leaf dimensions, we plotted leaf shrinkage against Ψ_{leaf}. We determined Ψ_{leaf} by summing the turgor pressure (Ψ_p) and solute potential (Ψ_s) estimated from the RWC using the fundamental leaf pressure-volume relationships (Bartlett et al., 2012b):

$$\Psi_p = -\pi_o - (\varepsilon(1 - RWC_i)) \quad (9)$$

$$\Psi_s = \pi_o + \left(\frac{\pi_{TLP} - \pi_o}{RWC_{TLP} - 1}\right)(RWC_i - 1) \quad (10)$$

$$\begin{aligned}\Psi_{leaf} &= \Psi_p + \Psi_s \\ &= \frac{(\varepsilon \times RWC_{TLP} + \pi_{TLP} - \varepsilon - \pi_o)RWC_i - \varepsilon \times RWC_{TLP} - \pi_{TLP} + \varepsilon + \pi_o}{RWC_{TLP} - 1}\end{aligned}$$
$$(11)$$

where π_o, π_{TLP}, and ε are as defined and RWC_{TLP} is the RWC at TLP (%). Values for these parameters were species means obtained from pressure-volume curves (Table II), previously published for the same plants for nine species (Scoffoni et al., 2008, 2011), and using additional data collected in this study for *Bauhinia galpinii*, *Platanus racemosa*, *Romneya coulteri*, and *Salvia canariensis* by measuring Ψ_{leaf} and RWC during progressive dehydration of initially rehydrated leaves ($n = 5$ leaves per species; Sack, 2010). We assumed a constant ε in Equation 9 (i.e. a linear decline of Ψ_p with RWC), although a

nonlinear decline has been reported in a number of species (Robichaux, 1984), indicating a variable ε according to leaf water status. However, a linear approximation of Ψ_p with RWC between full turgor and TLP often fits experimental data (including for our species) and is common in the literature (Koide et al., 2000; Bartlett et al., 2012b). Moreover, simulations showed that even declines of ε by severalfold between full turgor and TLP would in any case negligibly affect our calculations of Ψ_{leaf} using Equation 11 and the shrinkage traits calculated from it (data not shown).

Leaf Shrinkage Experiments: Determination of the Parameters of Leaf Shrinkage

To fully characterize leaf shrinkage with dehydration, we calculated 18 traits for each species (for derivations, see Table III; for data, see Supplemental Table S5), most of them relating to thickness shrinkage rather than area shrinkage, since we found area shrinkage to be much smaller before TLP than thickness shrinkage. The nine indices that we found to be most representative and useful were $PLT_{leaf,TLP}$, $PLT_{C,TLP}$, $PLT_{A,TLP}$, and $PLA_{leaf,TLP}$, PLT_{dry} and PLA_{dry}, and $dT_C/d\Psi$, $dT_A/d\Psi$, and $dT_{leaf}/d\Psi$ against Ψ_{leaf} between full turgor and TLP. These nine key indices were strongly correlated with nine additional parameters of leaf shrinkage that we determined for a comprehensive approach (Supplemental Table S4; Supplemental Materials and Methods S1).

Leaf Rehydration Experiments

We determined the recovery of leaf thickness for dehydrated leaves after rehydration using experiments on leaf discs (after Milburn, 1966). Shoots with healthy, mature sun-exposed leaves were collected from three individuals of 10 species, recut under pure water in the laboratory, and rehydrated overnight. The next day, leaves were placed underwater, and discs of 2 to 5 cm², depending on leaf size, were cut centrally between midrib and lamina ($n = 5$ per species), toweled dry, and measured for thickness and mass at full hydration. Next, shoot segments containing four leaves were recut under water and left to dehydrate on the bench or over a fan, such that leaves could be sampled either (1) between full turgor and TLP or (2) dehydrated past TLP. Then, each individual leaf on the shoot was sealed, still on the shoot, in a plastic sealable bag (Whirl-Pak; Nasco) that had been previously exhaled in. The shoot was then placed in a sealed plastic zipper bag with wet paper towels and left to equilibrate for at least 15 min and up to 2 h (as necessary for more dehydrated shoots), after which the Ψ_{leaf} was measured for the top and bottom leaves of the shoot using a pressure chamber (Plant Moisture Stress, model 1000), and if these differed by more than 0.2 MPa, the shoot was discarded. Leaf discs were cut from the two remaining leaves. As one treatment, leaf discs were cut under water to minimize the effect of embolism of the leaf xylem in dehydrated leaves in delaying or preventing rehydration and recovery of tissue dimensions. As a second treatment, using different shoots, leaf discs were cut in air to test whether the embolism of xylem and mesophyll cell walls would affect disc rehydration; these discs were then dipped in water to achieve a similar initial condition to those that were cut under water. Leaf discs were immediately placed in sealable plastic bags that had been previously exhaled in. Initial thickness and mass were measured for each disc using the digital calipers and balances described above. Discs were then submerged under ultrapure water with a height of 2 to 4 mm in a petri dish to rehydrate for 1 h, after which thickness and mass were measured. The percentage recovery in thickness was measured by dividing thickness after 1 h of rehydration by the average thickness at full hydration. If discs cut in air and under water did not differ significantly in their recovery, values were pooled.

Leaf Hydraulic Traits

We tested the correlation of leaf shrinkage parameters with leaf hydraulics traits and g_{min}. Values for leaf hydraulics traits were obtained from vulnerability curves determined using the evaporative flux method for 10 species (Scoffoni et al., 2011, 2012; Sack and Scoffoni, 2012): K_{leaf} at full turgor (K_{max}) and at TLP, the percentage decline of K_{leaf} at TLP, P_{50} and P_{80}, and $dK_{leaf}/d\Psi$. For g_{min}, we used values previously published for the same plants (Scoffoni et al., 2011).

Leaf Structural and Compositional Traits

We tested the correlation of shrinkage parameters with traits related to gross leaf morphology and composition averaged for five leaves per species (sampled

from at least three individuals). For the leaves used in the shrinkage experiments, we measured fully hydrated leaf area (cm^2) and thickness (mm), leaf dry mass per turgid leaf area (LMA; $g\,m^{-2}$) and leaf density ($g\,cm^{-3}$), calculated as LMA divided by leaf thickness. The fractions of leaf air, water, and solid were measured for four to 10 leaves per species by water infiltration into the airspaces (Roderick et al., 1999; Sack et al., 2003b). The airspace "thickness" in a dry leaf was obtained by multiplying the thickness of the dry leaf by (1 – solid fraction in the dry leaf), and the percentage airspace in a dry leaf was obtained by dividing its airspace thickness by the thickness of the dry leaf.

Leaf Water Storage Traits

SWC, C_{FT}, and C_{TLP} were obtained for each species from the pressure-volume curves described above (Sack et al., 2003b; Sack, 2010). Leaf area-specific capacitance at full turgor (C^*_{FT}) and C^*_{TLP} (in $mol\,m^{-2}\,MPa^{-1}$) were then calculated:

$$C^*_{FT} = C_{FT} \times SWC \times LMA \tag{12}$$

$$C^*_{TLP} = C_{TLP} \times SWC \times LMA \times RWC_{TLP} \tag{13}$$

Leaf Venation Traits

We tested the relationship of leaf shrinkage with published vein traits for the study plants (Scoffoni et al., 2011): major VLA (i.e. that of the first three branching orders of veins), minor VLA (i.e. that of higher vein-branching orders), total VLA (also known as "vein density"), and the ratio of major to minor VLA and free vein endings per area.

Statistics

We tested a priori hypotheses for the coordination of shrinkage parameters with pressure-volume parameters, hydraulic traits, and leaf structure and composition across species. As in previous studies using this approach (Brodribb et al., 2007; Waite and Sack, 2010; Scoffoni et al., 2011; Nardini et al., 2012), we did not correct individual correlations for multiple tests and present a correlation matrix of all traits only to illustrate the intercorrelative structure of all measured traits (Supplemental Table S3). We advise correction for multiple statistical tests before considering trait correlations that were not hypothesized a priori. Pearson coefficients were determined for both untransformed and log-transformed data, given that many relationships were nonlinear (Sokal and Rohlf, 1995). Spearman rank correlations were also determined, given that these are more robust in cases in which one or two outliers might drive a significant Pearson correlation (Sokal and Rohlf, 1995). For a conservative approach, we typically recognized relationships as significant only when $P < 0.05$ for both Spearman rank and Pearson correlations (r_s and r_p, respectively).

Partial correlation analyses (Sokal and Rohlf, 1995) were conducted when three variables of interest were intercorrelated across species. These analyses tested the relationship between two variables when the third is statistically held constant (implemented using the corpcor package in R; Schaefer et al., 2007).

Supplemental Data

The following materials are available in the online version of this article.

Supplemental Table S1. Parameters for simulated vulnerability.

Supplemental Table S2. Mean ± SE of shrinkage, rehydration, pressure-volume, hydraulic, water storage, leaf structure, and leaf venation traits.

Supplemental Table S3. Correlation matrix of 51 traits related to shrinkage, rehydration, pressure-volume curves, hydraulics, water storage, leaf structure, and venation across 14 species.

Supplemental Table S4. Symbols, terms, unit, derivation, and biological significance of 9 additional leaf thickness, area, and volume shrinkage traits this study.

Supplemental Table S5. Percent recovery in thickness after 1 h of rehydration for leaves of 10 species dehydrated before and past their turgor loss point.

Supplemental Table S6. Partial correlation analysis results.

Supplemental Results S1. Leaf shrinkage with dehydration: variation across diverse species of other shrinkage parameters and correlation with pressure volume parameters and cuticular conductance.

Supplemental Results S2. Leaf shrinkage with dehydration: variation between species of wet and dry habitats.

Supplemental Results S3. Recovery of leaf shrinkage in thickness.

Supplemental Discussion S1. The impact of leaf shrinkage on leaf hydraulic vulnerability: studies based on rehydration kinetics.

Supplemental Discussion S2. Mechanisms of leaf shrinkage: the role of the epidermis.

Supplemental Discussion S3. Resistance to leaf shrinkage: an important trait contributing to drought tolerance?

Supplemental Materials and Methods S1. Leaf shrinkage experiments: testing leaf responses to dehydration; determination of the other parameters of leaf shrinkage; and leaf structural and compositional traits.

LITERATURE CITED

Bartlett MK, Scoffoni C, Ardy R, Zhang Y, Sun S, Cao K, Sack L (2012a) Rapid determination of comparative drought tolerance traits: using an osmometer to predict turgor loss point. Methods in Ecology and Evolution **3:** 880–888

Bartlett MK, Scoffoni C, Sack L (2012b) The determinants of leaf turgor loss point and prediction of drought tolerance of species and biomes: a global meta-analysis. Ecol Lett **15:** 393–405

Blackman CJ, Brodribb TJ, Jordan GJ (2010) Leaf hydraulic vulnerability is related to conduit dimensions and drought resistance across a diverse range of woody angiosperms. New Phytol **188:** 1113–1123

Blonder B, Buzzard V, Simova I, Sloat L, Boyle B, Lipson R, Aguilar-Beaucage B, Andrade A, Barber B, Barnes C, et al (2012) The leaf-area shrinkage effect can bias paleoclimate and ecology research. Am J Bot **99:** 1756–1763

Bogue EE (1892) The shrinkage of leaves. Science **20:** 163

Boyer JS (1968) Relationship of water potential to growth of leaves. Plant Physiol **43:** 1056–1062

Boyer JS (1985) Water transport. Annu Rev Plant Biol **36:** 473–516

Brodribb TJ, Feild TS, Jordan GJ (2007) Leaf maximum photosynthetic rate and venation are linked by hydraulics. Plant Physiol **144:** 1890–1898

Burnham KP, Anderson DR (2002) Model Selection and Multimodel Inference, Ed 2. Springer, New York

Burnham KP, Anderson DR (2004) Multimodel inference: understanding AIC and BIC in model selection. Sociol Methods Res **33:** 261–304

Burquez A (1987) Leaf thickness and water deficit in plants: a tool for field studies. J Exp Bot **38:** 109–114

Canny M, Wong SC, Huang C, Miller C (2012) Differential shrinkage of mesophyll cells in transpiring cotton leaves: implications for static and dynamic pools of water, and for water transport pathways. Funct Plant Biol **39:** 91–102

Cochard H, Froux F, Mayr S, Coutand C (2004a) Xylem wall collapse in water-stressed pine needles. Plant Physiol **134:** 401–408

Cochard H, Nardini A, Coll L (2004b) Hydraulic architecture of leaf blades: where is the main resistance? Plant Cell Environ **27:** 1257–1267

Colpitts BG, Coleman WK (1997) Complex permittivity of the potato leaf during imposed drought stress. IEEE Trans Geosci Rem Sens **35:** 1059–1064

Crombie DS, Milburn JA, Hipkins MF (1985) Maximum sustainable xylem sap tensions in *Rhododendron* and other species. Planta **163:** 27–33

Cutler D (2005) Design in plants. *In* MW Collins, MA Atherton, JA Bryant, eds, Nature and Design. WIT Press, Southampton, UK, pp 95–124

Downey LA, Miller JW (1971) Rapid measurements of relative turgidity in maize (*Zea mays* L). New Phytol **70**: 555–560

Farquhar GD, Raschke K (1978) On the resistance to transpiration of the sites of evaporation within the leaf. Plant Physiol **61**: 1000–1005

Fellows RJ, Boyer JS (1978) Altered ultrastructure of cells of sunflower leaves having low water potentials. Protoplasma **93**: 381–395

Fensom DS, Donald RG (1982) Thickness fluctuations in veins of corn and sunflower detected by a linear transducer. J Exp Bot **33**: 1176–1184

Gardner WR, Ehlig CF (1965) Physical aspects of the internal water relations of plant leaves. Plant Physiol **40**: 705–710

Johansson I, Karlsson M, Shukla VK, Chrispeels MJ, Larsson C, Kjellbom P (1998) Water transport activity of the plasma membrane aquaporin PM28A is regulated by phosphorylation. Plant Cell **10**: 451–459

John GP, Scoffoni C, Sack L (2013) Allometry of cells and tissues within leaves. Am J Bot **100**: 1936–1948

Johnson DM, Meinzer FC, Woodruff DR, McCulloh KA (2009) Leaf xylem embolism, detected acoustically and by cryo-SEM, corresponds to decreases in leaf hydraulic conductance in four evergreen species. Plant Cell Environ **32**: 828–836

Jones HG (1973) Estimation of plant water status with beta-gauge. Agric Meteorol **11**: 345–355

Kadoya K, Kameda K, Chikaigumi S, Matsumoto K (1975) Studies on the hydrophysiological rhythms of Citrus trees. I. Cyclic fluctuations of leaf thickness and stem diameter of *Natsudaidai* seedlings. J Jpn Soc Hortic Sci **44**: 260–264

Kennedy JS, Booth CO (1958) Water relations of leaves from woody and herbaceous plants. Nature **181**: 1271–1272

Kim YX, Steudle E (2007) Light and turgor affect the water permeability (aquaporins) of parenchyma cells in the midrib of leaves of *Zea mays*. J Exp Bot **58**: 4119–4129

Koide RT, Robichaux RH, Morse SR, Smith CM (2000) Plant water status, hydraulic resistance and capacitance. *In* RW Pearcy, JR Ehleringer, HA Mooney, PW Rundel, eds, Plant Physiological Ecology: Field Methods and Instrumentation. Kluwer, Dordrecht, The Netherlands, pp 161–183

Lawlor DW, Cornic G (2002) Photosynthetic carbon assimilation and associated metabolism in relation to water deficits in higher plants. Plant Cell Environ **25**: 275–294

McBurney T (1992) The relationship between leaf thickness and plant water potential. J Exp Bot **43**: 327–335

McKown AD, Cochard H, Sack L (2010) Decoding leaf hydraulics with a spatially explicit model: principles of venation architecture and implications for its evolution. Am Nat **175**: 447–460

Meidner H (1952) An instrument for the continuous determination of leaf thickness changes in the field. J Exp Bot **3**: 319–325

Meidner H (1955) Changes in the resistance of the mesophyll tissue with changes in the leaf water content. J Exp Bot **6**: 94–99

Meidner H (1975) Water supply, evaporation, and vapor diffusion in leaves. J Exp Bot **26**: 666–673

Meidner H (1983) Our understanding of plant water relations. J Exp Bot **34**: 1606–1618

Milburn JA (1966) Conduction of sap. I. Water conduction and cavitation in water stressed leaves. Planta **69**: 34–42

Nardini A, Lo Gullo MA, Salleo S (2011) Refilling embolized xylem conduits: is it a matter of phloem unloading? Plant Sci **180**: 604–611

Nardini A, Pedà G, La Rocca N (2012) Trade-offs between leaf hydraulic capacity and drought vulnerability: morpho-anatomical bases, carbon costs and ecological consequences. New Phytol **196**: 788–798

Ogaya R, Peñuelas J (2006) Contrasting foliar responses to drought in *Quercus ilex* and *Phillyrea latifolia*. Biol Plant **50**: 373–382

Pammenter NW, Vander Willigen C (1998) A mathematical and statistical analysis of the curves illustrating vulnerability of xylem to cavitation. Tree Physiol **18**: 589–593

Pantin F, Monnet F, Jannaud D, Costa JM, Renaud J, Muller B, Simonneau T, Genty B (2013) The dual effect of abscisic acid on stomata. New Phytol **197**: 65–72

Pivovaroff A, Sharifi R, Scoffoni C, Sack L, Rundel P (2014) Making the best of the worst of times: traits underlying the combined shade and drought tolerance of *Ruscus aculeatus* and *Ruscus microglossum* (Asparagaceae). Funct Plant Biol **41**: 11–24

Robichaux RH (1984) Variation in the tissue water relations of two sympatric Hawaiian *Dubautia* species and their natural hybrid. Oecologia **65**: 75–81

Roderick ML, Berry SL, Saunders AR, Noble IR (1999) On the relationship between the composition, morphology and function of leaves. Funct Ecol **13**: 696–710

Rozema J, Arp W, Vandiggelen J, Kok E, Letschert J (1987) An ecophysiological comparison of measurements of the diurnal rhythm of the leaf elongation and changes of the leaf thickness of salt-resistant Dicotyledonae and Monocotyledonae. J Exp Bot **38**: 442–453

Sack L (2010) Leaf pressure-volume curve parameters. PrometheusWiki, http://www.publish.csiro.au/prometheuswiki/tiki-pagehistory.php?page=Leaf pressure-volume curve parameters&preview=10 (December 20, 2013)

Sack L, Cowan PD, Holbrook NM (2003a) The major veins of mesomorphic leaves revisited: tests for conductive overload in *Acer saccharum* (Aceraceae) and *Quercus rubra* (Fagaceae). Am J Bot **90**: 32–39

Sack L, Cowan PD, Jaikumar N, Holbrook NM (2003b) The 'hydrology' of leaves: co-ordination of structure and function in temperate woody species. Plant Cell Environ **26**: 1343–1356

Sack L, Frole K (2006) Leaf structural diversity is related to hydraulic capacity in tropical rain forest trees. Ecology **87**: 483–491

Sack L, Holbrook NM (2006) Leaf hydraulics. Annu Rev Plant Biol **57**: 361–381

Sack L, Melcher PJ, Liu WH, Middleton E, Pardee T (2006) How strong is intracanopy leaf plasticity in temperate deciduous trees? Am J Bot **93**: 829–839

Sack L, Scoffoni C (2012) Measurement of leaf hydraulic conductance and stomatal conductance and their responses to irradiance and dehydration using the Evaporative Flux Method (EFM). J Vis Exp **70**: e4179

Sack L, Streeter CM, Holbrook NM (2004) Hydraulic analysis of water flow through leaves of sugar maple and red oak. Plant Physiol **134**: 1824–1833

Sack L, Tyree MT, Holbrook NM (2005) Leaf hydraulic architecture correlates with regeneration irradiance in tropical rainforest trees. New Phytol **167**: 403–413

Saini BC, Rathore TR (1983) Adaptation of beta-ray gauge technique for measurement of water deficit of intact rice leaves. Biol Plant **25**: 326–330

Salleo S, Lo Gullo MA, Raimondo F, Nardini A (2001) Vulnerability to cavitation of leaf minor veins: any impact on leaf gas exchange? Plant Cell Environ **24**: 851–859

Sancho-Knapik D, Alvarez-Arenas TG, Peguero-Pina JJ, Fernández V, Gil-Pelegrín E (2011) Relationship between ultrasonic properties and structural changes in the mesophyll during leaf dehydration. J Exp Bot **62**: 3637–3645

Sancho-Knapik D, Gómez Alvarez-Arenas T, Peguero-Pina JJ, Gil-Pelegrín E (2010) Air-coupled broadband ultrasonic spectroscopy as a new non-invasive and non-contact method for the determination of leaf water status. J Exp Bot **61**: 1385–1391

Schaefer J, Opgen-Rhein R, Strimmer K (2007) corpcor: efficient estimation of covariance and (partial) correlation. R package version 1.4.7. http://cran.r-project.org/web/packages/corpcor (December 20, 2013)

Scoffoni C, McKown AD, Rawls M, Sack L (2012) Dynamics of leaf hydraulic conductance with water status: quantification and analysis of species differences under steady state. J Exp Bot **63**: 643–658

Scoffoni C, Pou A, Aasamaa K, Sack L (2008) The rapid light response of leaf hydraulic conductance: new evidence from two experimental methods. Plant Cell Environ **31**: 1803–1812

Scoffoni C, Rawls M, McKown A, Cochard H, Sack L (2011) Decline of leaf hydraulic conductance with dehydration: relationship to leaf size and venation architecture. Plant Physiol **156**: 832–843

Seelig HD, Stoner RJ, Linden JC (2012) Irrigation control of cowpea plants using the measurement of leaf thickness under greenhouse conditions. Irrig Sci **30**: 247–257

Shatil-Cohen A, Attia Z, Moshelion M (2011) Bundle-sheath cell regulation of xylem-mesophyll water transport via aquaporins under drought stress: a target of xylem-borne ABA? Plant J **67**: 72–80

Sheriff DW, Meidner H (1974) Water pathways in leaves of *Hedera helix* L and *Tradescantia virginiana* L. J Exp Bot **25**: 1147–1156

Sokal RR, Rohlf FJ (1995) Biometry: The Principles and Practice of Statistics in Biological Research, Ed 3. WH Freeman, New York

Syvertsen JP, Levy Y (1982) Diurnal changes in citrus leaf thickness, leaf water potential and leaf to air-temperature difference. J Exp Bot **33**: 783–789

Tang AC, Boyer JS (2007) Leaf shrinkage decreases porosity at low water potentials in sunflower. Funct Plant Biol **34**: 24–30

Tyree MT, Cameron SI (1977) New technique for measuring oscillatory and diurnal changes in leaf thickness. Can J For Res **7**: 540–544

Tyree MT, Hammel HT (1972) Measurement of turgor pressure and water relations of plants by pressure bomb technique. J Exp Bot **23**: 267–282

Tyree MT, Zimmermann MH (2002) Xylem Structure and the Ascent of Sap. Springer, Berlin

Waite M, Sack L (2010) How does moss photosynthesis relate to leaf and canopy structure? Trait relationships for 10 Hawaiian species of contrasting light habitats. New Phytol **185**: 156–172

Wylie RB (1943) The role of the epidermis in foliar organization and its relations to the minor venation. Am J Bot **30**: 273–280

Zimmermann MH (1978) Hydraulic architecture of some diffuse-porous trees. Can J Bot **56**: 2286–2295